ORIGINAL ARTICLE

Modeling Proximal Tubule Cell Homeostasis: Tracking Changes in Luminal Flow

Alan M. Weinstein[a,*], Eduardo D. Sontag[b]

[a]*Department of Physiology and Biophysics, Weill Medical College of Cornell University, 1300 York Avenue, New York, NY 10021, USA*
[b]*Department of Mathematics, Rutgers University, New Brunswick, USA*

Abstract During normal kidney function, there are routinely wide swings in proximal tubule fluid flow and proportional changes in Na^+ reabsorption across tubule epithelial cells. This "glomerulotubular balance" occurs in the absence of any substantial change in cell volume, and is thus a challenge to coordinate luminal membrane solute entry with peritubular membrane solute exit. In this work, linear optimal control theory is applied to generate a configuration of regulated transporters that could achieve this result. A previously developed model of rat proximal tubule epithelium is linearized about a physiologic reference condition; the approximate linear system is recast as a dynamical system; and a Riccati equation is solved to yield the optimal linear feedback that stabilizes Na^+ flux, cell volume, and cell pH. The first observation is that optimal feedback control is largely consigned to three physiologic variables, cell volume, cell electrical potential, and lateral intercellular hydrostatic pressure. Parameter modulation by cell volume stabilizes cell volume; parameter modulation by electrical potential or interspace pressure act to stabilize Na^+ flux and cell pH. This feedback control is utilized in a tracking problem, in which reabsorptive Na^+ flux varies over a factor of two, in order to represent a substantial excursion of glomerulotubular balance. The resulting control parameters consist of two terms, an autonomous term and a feedback term, and both terms include transporters on both luminal and peritubular cell membranes. Overall, the increase in Na^+ flux is achieved with upregulation of luminal Na^+/H^+ exchange and Na^+–glucose cotransport, with increased peritubular Na^+–$3HCO_3^-$ and K^+–Cl^- cotransport, and with increased Na^+, K^+–ATPase activity. The configuration of activated transporters emerges as a testable hypothesis of the molecular basis for glomerulotubular balance. It is suggested that the autonomous control component at each cell membrane could represent the cytoskeletal effects of luminal flow.

Keywords Cell volume regulation · Cell pH regulation · Proximal tubule · Glomerulotubular balance

---

*Corresponding author.
E-mail address:* alan@nephron.med.cornell.edu (Alan M. Weinstein).

1. Modeling proximal tubule cell homeostasis: tracking changes in luminal flow

All transporting epithelial cells routinely face the challenge of varying solute throughput, while avoiding lethal changes in cell volume or composition (Schultz, 1981, 1992). In the proximal tubule of the kidney, this challenge presents itself with the tubular response to minute-by-minute variations in glomerular filtration (the delivered load to the tubule), for which solute and water reabsorption varies proportionally (Schnermann et al., 1968). This "glomerulotubular balance" derives from both peritubular capillary and luminal factors (Gertz and Boylan, 1973; Haberle and von Baeyer, 1983; Weinstein, 1990). The most important luminal factor is a direct effect of axial flow velocity on transport (Wilcox and Baylis, 1985; Romano et al., 1998), and along with its impact on sodium reabsorption, luminal flow has been found to influence the transport of glucose (Knight et al., 1980), bicarbonate (Chan et al., 1982; Alpern et al., 1983; Liu and Cogan, 1988), and chloride (Green et al., 1981; Wong et al., 1995). Insight into the mechanism underlying flow-dependent transport came with the demonstration that increases in axial flow velocity recruit new Na^+/H^+ transporters into the luminal membrane (Preisig, 1992; Maddox et al., 1992). With respect to the afferent signal, Guo et al. (2000) proposed that the proximal tubule brush border microvilli serve as the flow sensor, and that the drag force on each microvillus produced torque on its actin filament core that was transmitted to the underlying cytoskeleton. This hypothesis received support from the experiments of Du et al. (2004, 2006) who studied mouse proximal tubules perfused in vitro, and found that over a five-fold variation of luminal perfusion rate, there was a predicted 2-fold variation in microvillous torque, which scaled identically with Na^+ and HCO_3^- reabsorption. Disabling the cytoskeletal response (using cytochalasin), eliminated the flow effect on transport. In those experiments, luminal flow impacted H^+ secretion via both the Na^+/H^+ antiporter and the H^+–ATPase, although the full extent of luminal membrane transporters influenced by microvillous torque has not been delineated. With respect to flow-dependent modulation of solute exit from tubule cells across basolateral (or peritubular) membranes, there are two possibilities: One is activation of peritubular membrane transporters according to feedback signals for homeostasis of cell volume and composition (Lang et al., 1998a, 1998b). The other possibility is a direct effect of flow (perhaps via the cytoskeleton) on peritubular membrane transporters themselves. The peritubular impact of luminal flow has not been addressed in experimental studies.

The proximal tubule of the rat has been the most intensively modeled nephron segment, and in these models the luminal membrane Na^+/H^+ exchanger emerged as the most important determinant of proximal Na^+ reabsorption (Weinstein, 1992). These models were later used to examine coordination of luminal and peritubular transport pathways that could preserve cell volume and composition during variations of Na^+ reabsorption. Although experimental studies had focused on peritubular membrane K^+ channels as important for homeostasis, the model calculations identified two other peritubular exit pathways, K^+–Cl^- and Na^+–$3HCO_3^-$ cotransporters, as likely to be of greater impact (Weinstein, 1996). Indeed, it proved impossible to simulate the range of proximal tubule Na^+ transport observed with variation in luminal flow rates, without coordinate changes in both luminal and peritubular transporters (Weinstein et al., 2007). With respect to model performance, an important observation was that over a broad range of input conditions, the steady-state output of the proximal tubule model could be approximated by its linearization (Weinstein, 1999). This linearization allowed systematic exploration of

state variable control of transporter activity during cell volume challenges, and identified volume-dependent K^+–Cl^- or Na^+–$3HCO_3$ cotransport as mechanisms which could enhance Na^+ through-put while preserving cell volume. Linearization of the time-dependent proximal tubule cell model proved to be more involved. Ultimately, the system of 10 differential equations and 21 algebraic equations for 31 model variables was approximated by a 9-dimensional linear dynamical system, along with a linear map into the original space of physiologic variables (Weinstein, 2004). This linear approximation reproduced the full model behavior in a physiologically useful neighborhood of the reference conditions. Cost functions on trajectories were naturally formulated in terms of the physiologic variables (e.g. time for cell volume recovery), and then translated into cost functions for the dynamical system. This permitted formulation of an algebraic Riccati equation to identify an ensemble of controllers that constituted optimal state feedback for the dynamical system. When translated back into the physiological variables, the optimal controller contained expected components (i.e. reliance on volume-dependent K^+–Cl^- cotransport), as well as unanticipated controllers of uncertain significance (e.g. volume-dependent luminal membrane Na^+–glucose or Na^+–phosphate cotransport). This approach provided a means of relating cellular homeostasis to optimization of a dynamical system.

The problem posed by glomerulotubular balance is for proximal tubule Na^+ reabsorption to vary in parallel with changes in filtered load, and this is to occur with minimal derangement in cell volume and composition. To achieve this, the optimal control approach (Weinstein, 2004) is now extended with the formulation of a tracking problem, in which variation in proximal tubule cell Na^+ flux, over a factor of two, is asked to follow a specified time course. As previously, the time-dependent epithelial model is linearized as a dynamical system that incorporates the possibility of feedback control of model parameters by the state variables. For the tracking problem, luminal membrane Na^+ flux computed in the full proximal tubule model must be approximated as a linear function of the state variables of the dynamical system. Then, one cost of a trajectory is the difference between predicted and desired Na^+ fluxes. Additional trajectory costs are the derangement in cell volume and solute concentrations, as well as the magnitude of the parameter modulation. This problem is formulated as a Riccati differential equation that is a natural extension of the algebraic Riccati equation (Sontag, 1998). The solution of this equation provides model parameters as a function of time with two components: a feedback component, in which transport coefficients are a linear function of the state variables, and an autonomous (or feed-forward) component, in which transport coefficients are functions of time. The salient observations from these calculations are that both feedback and autonomous components of parameter variation are substantial. Furthermore, both parameter components involve transporters on both luminal and peritubular cell membranes. When the linear feedback law is translated into control by physiological variables, and the autonomous parameter variation is taken as input into the full epithelial model, the proximal tubule cell model can reproduce the desired variation in Na^+ flux with minor derangements in cell volume and composition.

2. Proximal tubule model

Figure 1 shows the proximal tubule cell as used previously (Weinstein, 1992, 2004). The model consists of compliant cellular and lateral intercellular compartments, with 12 model

PCT Transport Pathways
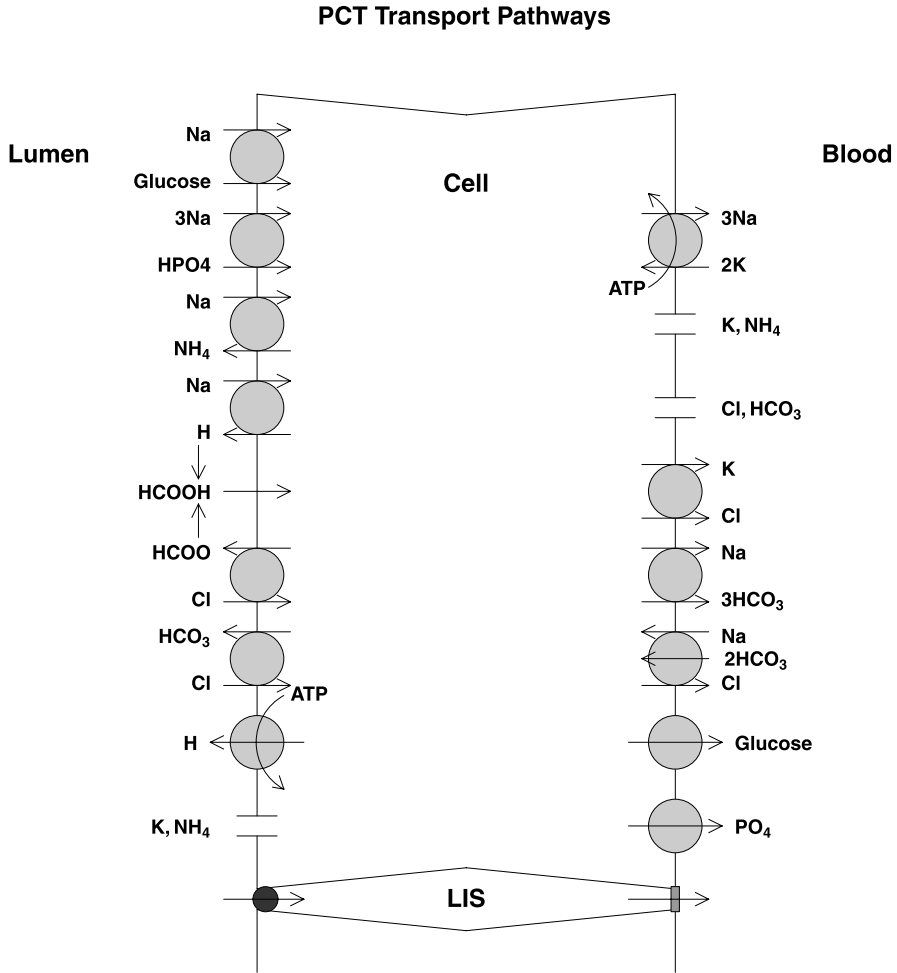
Fig. 1 Schematic of the proximal tubule epithelium consisting of compliant cellular and lateral interspace (LIS) compartments. There are 12 permeant solute species: Na^+, K^+, Cl^-, HCO_3^-, $HPO_4^=$, $H_2PO_4^-$, glucose, urea, HCO_2^-, H_2CO_2, NH_3, and NH_4^+, plus a cytosolic impermeant. Within the cell membranes are channels (for K^+ and Cl^-), facilitated transporters (for glucose and phosphate), cotransporters and antiporters, and ATP-driven ion pumps (H^+–ATPase and Na, K–ATPase). The LIS is separated from the lumen by a tight junction, and from the peritubular fluid by a basement membrane, both with finite solute permeabilities.

solute species: Na^+, K^+, Cl^-, HCO_3^-, $HPO_4^=$, $H_2PO_4^-$, glucose, urea, HCO_2^-, H_2CO_2, NH_3, and NH_4^+. The vector of model unknowns, u, includes the cell PD, the concentration of the cellular impermeant anion (equivalently, the cell volume), the 12 cytosolic solute concentrations, and the concentrations of an impermeant cellular buffer pair. In addition to these 16 cytosolic variables, there are 14 lateral intercellular space (LIS) variables. (Within the LIS, there are no impermeants, and hydrostatic pressure provides the model

variable which insures volume conservation.) H^+ concentration is not treated as a distinct solute within cell or LIS, and the (fixed) pCO_2 to HCO_3^- ratio is used in the calculation of buffer equilibria. The LIS is a compartment whose volume is about 10% that of the cell, and is separated from the luminal solution by the tight junction, and from the peritubular solution by the basement membrane. The tight junction solute permeabilities are more than an order of magnitude greater than those of the cell membranes, and the basement membrane permeabilities are about an order of magnitude greater than those of the tight junction. Although solute concentrations within the LIS may be different from those of either bath, the small size and high permeabilities of the bounding membranes permits the simplification that LIS concentrations are always at steady-state. One additional model variable is the transepithelial electrical potential, which derives from the zero-net current constraint on the net fluxes. Figure 1 displays most of the important transport pathways across the luminal and peritubular cell membranes. Corresponding to each of these pathways, is a single model parameter which may be identified as the effective membrane permeability or density of the transporter, and it is these parameters which comprise the parameter vector, p.

The model compartments are denoted by a single character, lumen (M), cell (I), interspace (E), and peritubular bath or capillary (S), and the separating membranes by two characters, luminal cell membrane (MI), lateral cell membrane (IE), basal cell membrane (IS), tight junction (ME), and interspace basement membrane (ES). The order of the two characters indicates the positive direction for mass flow. For the uncoupled permeation of neutral solutes across membranes, a Fick law is utilized, and for permeation of charged species, there is a Goldman equation, in which a single permeability coefficient characterizes the pathway. For example, the flux, $J_{IS}(K^+)$, through the peritubular K^+ channel is given by

$$J_{IS}(K^+) = H_{IS}(K^+)\zeta_{IS}(K^+)\left[\frac{C_I(K^+) - C_S(K^+)e^{-\zeta_{IS}(K^+)}}{1 - e^{-\zeta_{IS}(K^+)}}\right], \tag{1}$$

$$\zeta_{IS}(K^+) = \frac{F}{RT}\psi_{IS}, \tag{2}$$

in which C_I and C_S are the K^+ concentrations in cell and peritubular bath, $\psi_{IS} = \psi_I - \psi_S$ is the electrical potential difference across the basal cell membrane, and $H_{IS}(K^+)$ is the permeability coefficient for this pathway. With the exception of the Na^+/H^+ antiporter of the luminal membrane, all of the coupled solute transport in this model has been represented according to linear nonequilibrium thermodynamics, so that solute permeation rates are proportional to the electrochemical driving force of the aggregate species, again with a single permeation coefficient. For example, the flux through the peritubular K^+–Cl^- cotransporter is given by

$$\begin{pmatrix} J_{IS}(K^+) \\ J_{IS}(Cl^-) \end{pmatrix} = L_{KCl}\begin{bmatrix} 1 & 1 \\ 1 & 1 \end{bmatrix}\begin{pmatrix} \bar{\mu}_{IS}(K^+) \\ \bar{\mu}_{IS}(Cl^-) \end{pmatrix}, \tag{3}$$

$$\bar{\mu}_{IS}(i) = RT\ln\big(C_I(i)/C_S(i)\big) + z_i F\psi_{IS}, \tag{4}$$

where $\bar{\mu}_{IS}(i)$ is the electrochemical potential difference of species i across the basal cell membrane. For this cotransporter, L_{KCl} is the rate coefficient identified as its permeability.

With respect to the Na^+/H^+ exchanger, a kinetic model for this transporter has been incorporated into the epithelial model, and the density of this transporter within the luminal membrane is used as an element of the parameter vector. Similarly, both metabolically driven pumps of this model, the peritubular Na^+, K^+–ATPase and the luminal H^+–ATPase, also have specified maximal fluxes, which appear in the parameter vector. The Na^+, K^+–ATPase transports 3 Na^+ in exchange for 2 K^+ across basal and lateral cell membranes, and the expression used for the Na^+ flux, J_{IS}^{act}:

$$J_{IS}^{act}(Na^+) = \left[J_{IS}^{act}(Na^+)\right]_{max} \left[\frac{C_I(Na^+)}{C_I(Na^+) + K_{Na}}\right]^3 \left[\frac{C_S(K^+)}{C_S(K^+) + K_K}\right]^2. \tag{5}$$

The luminal membrane proton flux through its ATPase is

$$J_{MI}(H^+) = -L_0(H^+)\left[\frac{1}{1 + \exp[\xi(\bar{\mu}_{MI}(H^+) - \bar{\mu}_{1/2})]}\right], \tag{6}$$

where L_0 is a maximal flux, $\bar{\mu}_{1/2}$ is the proton potential difference at which flux is half maximal, and ξ is a steepness coefficient.

Thus, with 24 permeabilities (12 model solutes crossing luminal and peritubular cell membranes), 8 coupled transporters, and 2 pumps, there are 34 possible elements to p. Of these, 10 membrane permeabilities are sufficiently small to be inconsequential, so that in the calculations that follow only 24 model parameters are examined. (The elements of p are displayed as the rows of Table 3.) In the baseline model, all of these parameters are unmodulated by cytosolic conditions, with the one exception of the luminal membrane Na^+/H^+ exchanger, whose density is increased by cellular acidosis. In principle, the parameter increments, $p(i)$, will be functions of the perturbations of the model variables, $u(j)$. What is done here to simulate regulated transporters within the full proximal tubule model, is to rely on linear dependence relations

$$\frac{p(i)}{p_{ss}(i)} = \alpha(i, j) \cdot \frac{u(j)}{u_{ss}(j)}, \tag{7}$$

in which the fractional change in element i of p (compared with the steady-state parameter, $p_{ss}(i)$) is proportional to the fractional change in element j of u (compared with the steady-state value of the variable, $u_{ss}(j)$), with sensitivity, $\alpha(i, j)$.

The epithelial model equations consist of conservation relations, pH equilibria for the reactive species, and electroneutrality, formulated for both cell and lateral intercellular space. With reference to the cell, export of volume, Q_v, and export of solute species i, Q_i, is represented

$$Q_v = J_{IE}(v) + J_{IS}(v) - J_{MI}(v), \tag{8}$$

$$Q_i = J_{IE}(i) + J_{IS}(i) - J_{MI}(i). \tag{9}$$

The generation of volume and solute (s_v and s_i) results in either new cellular mass or export from the cell:

$$s_v = \frac{dV_I}{dt} + Q_v, \qquad s_i = \frac{d[C_I(i)V_I]}{dt} + Q_i. \tag{10}$$

With this notation, mass conservation requires zero generation of volume and zero generation for the non-reactive solute species,

$$0 = s_v, \qquad 0 = s_i, \quad i = \text{Na}^+, \text{K}^+, \text{Cl}^-, \text{glucose, urea} \tag{11}$$

conservation of total buffer for transported and impermeant buffer pairs,

$$0 = s_{\text{HPO}_4} + s_{\text{H}_2\text{PO}_4} = s_{\text{HCO}_3} + s_{\text{H}_2\text{CO}_2} = s_{\text{NH}_3} + s_{\text{NH}_4} = s_{\text{B}^-} + s_{\text{HB}} \tag{12}$$

and electroneutrality for all of the buffer reactions (conservation of protons),

$$0 = \sum_i z_i s_i, \tag{13}$$

where z_i is the valence of species i. The algebraic relations of the model include the pH equilibria of the 4 buffer pairs,

$$\text{pH} = \text{pK} + \log_{10} \frac{\text{Base}^-}{\text{HBase}} \tag{14}$$

and electroneutrality

$$0 = \sum_i z_i C_{\text{I}}(i). \tag{15}$$

In (12), the conservation relation for the impermeant buffer contains no trans-membrane flux terms, so that this equation is immediately integrated and treated as an algebraic equation. Thus, for the cell there are 16 model equations (10 differential equations plus 6 algebraic equations); for the lateral interspace (without an impermeant buffer) an additional 14; and one equation for zero net current for the sum of the fluxes across transcellular and paracellular pathways. For the calculations of this paper, the model differential equations were solved using a first-order implicit scheme. The model parameters are those previously published (Weinstein, 1992), as updated with the inclusion of ammonia permeabilities (Weinstein, 1994).

3. Model analysis

3.1. Linearization

Linearization of the proximal tubule model is identical to that described previously (Weinstein, 2004). In brief, the system of 31 model equations is of the form

$$0 = \phi(u', u + u_{\text{ss}}, p + p_{\text{ss}}), \tag{16}$$

in which u and p are deviations from their reference values, u_{ss} and p_{ss}. p_{ss} represents a reference parameter set, and u_{ss} is the steady state solution of the model equations after setting $u' = 0$,

$$0 = \phi(0, u_{\text{ss}}, p_{\text{ss}}). \tag{17}$$

In addition to the reference condition, the solution of (17) using Newton's method also yields the Jacobian at the reference,

$$R = \frac{\partial \phi}{\partial u_{ss}}, \qquad 31 \times 31. \tag{18}$$

At this reference, the dependence of ϕ on p was obtained by incrementing each of the 24 parameters of interest by 1% of its baseline value and recomputing ϕ

$$Q = \frac{\partial \phi}{\partial p_{ss}}. \tag{19}$$

For the time-dependent model, the system function, ϕ, consists of 10 differential equations, corresponding to mass conservation within the cell, and 21 algebraic equations, corresponding to pH equilibria and electroneutrality, and to lateral interspace conditions. Thus the derivative,

$$S = -\frac{\partial \phi}{\partial u'} \tag{20}$$

has 21 rows with all zero entries, and 10 nontrivial rows, whose entries can be written in closed form. Computation of the matrices R, Q, and S (all evaluated at u_{ss}), yields a linear model of the form

$$Su' = Ru + Qp. \tag{21}$$

As illustrated in the upper portion of Fig. 2, the algebraic equations constrain model trajectories to a manifold within the 31-dimensional u-space. The linearized system constrains trajectories to the tangent subspace at u_{ss}. In order to cast the model as a dynamical system, it is necessary to identify this subspace, and this was the principal focus of the earlier work (Weinstein, 2004). In that paper, it was shown that the tangent subspace had dimension 9, so that the dynamical system could be defined on the 9-dimensional x-space, illustrated in the lower portion of Fig. 2. With three applications of the singular value decomposition, the system (21) can be brought to the form

$$x' = Ax + Bp, \tag{22}$$

in which A is the system matrix, p is the vector of parameter displacements shown in (21), and B translates the effect of parameter perturbations to the system variables. The relevant tangent space within the u-coordinates is given by

$$u = Cx, \tag{23}$$

in which C is an orthogonal matrix of dimension 31×9, so that $C^t C = I$. With $x = C^t u$, the composite map CC^t is a projection onto the tangent space at u_{ss}. The same parameter vector, p appears in both systems (21) and (22), so that the matrix B must satisfy

$$B = AC^t R^{-1} Q. \tag{24}$$
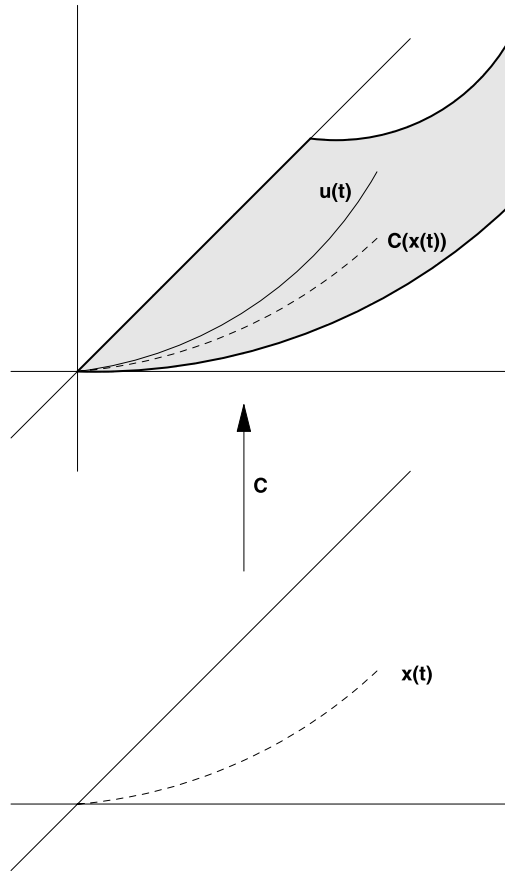
Fig. 2 The algebraic equations of the model constrain model trajectories to a manifold (shaded region) within the 31-dimensional u-space (upper coordinates). The linear dynamical system is formulated on the 9-dimensional x-space (lower coordinates). The isometry, C, maps trajectories $x(t)$ into a subspace of u, tangent to the manifold at the origin.

If a feedback matrix, F, is identified for the dynamical system to calculate p as a function of x, namely $p = Fx$, then

$$x' = Ax + Bp = (A + BF)x. \tag{25}$$

In view of the relation, $p = Fx = FC^tCx = (FC^t)u$, the corresponding feedback on the space of physiologic variables, u, is $P = FC^t$, and

$$u' = (R + QP)u = (R + QFC^t)u. \tag{26}$$

3.2. Cost of a trajectory

Suppose that in the u-coordinates M is an $n \times n$ symmetric non-negative matrix, which defines the cost, $J(t)$, of trajectories $u(s)$ over the interval $[0, t]$

$$J(t) = \int_0^t \big(u(s), Mu(s)\big)\, ds \tag{27}$$

or over the full trajectory by

$$J = \int_0^\infty \big(u(s), Mu(s)\big)\, ds \tag{28}$$

then the natural cost, N, to apply to a trajectory in the dynamical system, $x(t)$, is

$$N = C^t M C. \tag{29}$$

In the prior work (Weinstein, 2004), M was either the identity matrix (for which the trajectory cost could be considered the time to recovery), or a diagonal matrix with a single nonzero entry corresponding to the cellular impermeant (trajectory cost as a time-averaged volume displacement). In the present work, the costs of interest will be cell volume, cell HCO_3^- concentration, and cell Na^+ flux (i.e. Na^+ entry across the luminal cell membrane, $J_{MI}(Na^+)$). The estimation of $J_{MI}(Na^+)$ comes as part of the model linearization calculation of the matrix, R (18), which includes the computation of $J_{MI}(Na^+)$ with perturbation of each component of u:

$$m_{JNa} = \frac{\partial J_{MI}(Na^+)}{\partial u}. \tag{30}$$

Thus (m_{JNa}) is a row vector of dimension 31, and the matrix, M_{JNa}, defined by

$$M_{JNa} = (m_{JNa})^t (m_{JNa}) \tag{31}$$

can be used to identify a cost for deviations from reference in luminal Na^+ entry. Addition of M_{JNa} to the cost matrices for cell volume or HCO_3^- concentration provide a means of stabilizing Na^+ flux along with the state variables.

In order to formulate an optimization problem, parameter modulation must come at a price, namely $(p(t), Kp(t))$, in which K is a symmetric positive-definite matrix. Thus when parameter variation is solely via the feedback control matrix, F, the parameter cost is $(x(t), F^t K F x(t))$, and the total cost of a trajectory is,

$$J(t) = \int_0^t \big(x(s), (N + F^t K F)x(s)\big)\, ds. \tag{32}$$

In the prior work (Weinstein, 2004), the matrix K was taken as a positive multiple of the identity matrix. For that choice, the cost for varying all parameters was equal, and biased the solution toward variation of the smaller permeabilities. In the present work, the matrix K is a positive multiple of the diagonal matrix whose entries are $(1/p_{ss}(i))^2$, so that fractional changes in each parameter are weighted equally.

The dynamical system referenced in (32) has the system matrix $A + BF$ (25). Over a whole trajectory ($t \to \infty$), the cost may be determined by first solving the Lyapunov equation

$$(A + BF)^t Y + Y(A + BF) = -F^t K F - N \tag{33}$$

for a unique symmetric matrix, Y. For a trajectory starting at x_0, the total cost is then $J = (x_0, Y x_0)$. (For derivation, see (3.34)–(3.36) in Weinstein, 2004). In the case that F and Y also satisfy

$$F = -K^{-1} B^t Y \tag{34}$$

then Y satisfies the algebraic Riccati equation

$$A^t Y + Y A - Y B K^{-1} B^t Y + N = 0. \tag{35}$$

In that case, F provides optimal control, and J is minimal for all choices of x_0 (Wonham, 1985). Solution of the two simultaneous equations (33) and (34), can proceed iteratively: given a guess for F, provided that $A + BF$ is stable, (33) is solved for Y, and this is used in (34) to update F. This iterative procedure is in fact a Newton iteration, with quadratic convergence (Kleinman, 1968).

3.3. The tracking problem

Under normal circumstances, the proximal tubule cell is not confronted with the problem of recovery from a displacement. Rather, reabsorption of Na^+ from the luminal solution follows changes in axial flow rate, so that cellular Na^+ reabsorption remains roughly proportional to Na^+ delivery, and this should be accomplished with minimal disturbance to the cell volume and composition. This consideration motivates formulation of a tracking problem, in which Na^+ reabsorption is a specified function. Following the approach of Sontag (1998), there is a natural extension of the optimization process outlined above to the problem of achieving time-dependent model output. Denote the signal to be tracked as $r(t)$, a vector of dimension p, and M_r a $p \times n$ matrix that can be used to define a tracking error, $e(t)$:

$$e(t) = M_r u(t) - r(t) = M_r C x(t) - r(t). \tag{36}$$

As a specific example, the tracking signal will be of the form $r(t) = (0, 0, v(t))^t$, so that one asks that cytosolic volume and HCO_3^- remain constant, while luminal membrane Na^+ flux follows a specified function, $v(t)$, intended to monitor axial fluid flow along the proximal tubule. In this problem, M_r can have 3 rows

$$M_r = \begin{bmatrix} m_{\text{Imp}} \\ m_{\text{HCO}_3} \\ m_{\text{JNA}} \end{bmatrix}, \tag{37}$$

in which m_{JNa} is the luminal Na$^+$ flux, as defined in (30), and m_{Imp} and m_{HCO_3} are vectors with a single positive entry corresponding to the cell impermeant or cell HCO$_3^-$ concentration. For this example, the products

$$M = M_r^t M_r \quad and \quad N = C^t M_r^t M_r C \tag{38}$$

define cost functions for the algebraic Riccati equation that tax deflections in cell volume, cell HCO$_3^-$, and luminal Na$^+$ flux.

Solution of the system (33) and (34) with the cost function of (38) provides an optimal feedback, F. This is used to formulate an auxiliary final value problem in β, over the interval $[0, T]$:

$$\frac{d\beta}{dt} = -(A + BF)^t \beta + C^t M_r^t r(t), \quad \beta(T) = 0. \tag{39}$$

Note that β does not depend on the initial condition of the problem, but on a final value. This equation derives from the optimization problem with a finite time horizon, and solution of a Riccati Differential Equation (Sontag, 1998, pp. 371–375). Once β is determined, the optimal trajectory on $[0, T]$, $x(t)$ is defined by

$$\frac{dx}{dt} = (A + BF)x - BK^{-1}B^t \beta(t), \quad x(0) = x_0 \tag{40}$$

and the optimal parameter control is

$$p(t) = Fx(t) - K^{-1}B^t \beta(t). \tag{41}$$

For this problem, the parameter deviation is the sum of two terms: the first given by the optimal feedback controller, and the second is an autonomous term specified by the solution of an auxiliary problem that incorporates the tracking signal $r(t)$ and looks forward to the time interval end point.

4. Model calculations

In the present work, the transport parameters employed in the full model are identical to those used previously (Weinstein, 2004). In the previous work, calculations examined perturbations from a single reference state, in which the model epithelium was bathed on both luminal and peritubular sides by solutions of equal composition, suggestive of early proximal tubule fluid. In the present work, a second reference point is considered, in which luminal glucose has been depleted by 90% (5.0 to 0.5 mM) and luminal HCO$_3^-$ has been reduced from 24 to 15 mM (with a compensatory increase in luminal Cl$^-$, and shifting of the other luminal buffer pairs: phosphate, formate, and ammonia), suggestive of mid-proximal tubule fluid. With this composition, Na$^+$ flux through the powerful Na$^+$–glucose cotransporter is blunted, and the impact of the Na$^+$/H$^+$ exchanger is enhanced. Table 1 displays the reference values of cellular variables and selected solute fluxes for the model epithelium at this second reference point. In comparison with the early proximal solution, the mid-proximal tubule cell is hyperpolarized by 4.6 mV and cytosolic glucose has decreased from 16.7 to 6.4 mM, due to the decrease in electrogenic Na$^+$–glucose entry

Table 1 Model solutions for mid-proximal tubule cell

	Reference	$Na^+/H^+ \times 2.0$
Cell volume, cm^3	0.90×10^{-3}	1.11×10^{-3}
Peritubular potential, mV	-60.7	-58.6
Transepithelial PD, mV	1.47	1.68
Interspace pressure, mmHg	11.7	12.4
Concentrations, mM		
Na^+	17.3	18.4
K^+	143.1	141.9
Cl^-	15.2	21.2
HCO_3^-	24.2	29.8
$HPO_4^=$	9.97	11.58
$H_2PO_4^-$	3.10	2.93
Glucose	10.11	9.65
Urea	4.93	4.92
HCO_2^-	0.534	0.692
H_2CO_2	0.151×10^{-3}	0.159×10^{-3}
NH_3	0.219×10^{-3}	0.206×10^{-3}
NH_4^+	0.152	0.116
pH	7.308	7.397
Buf^-	31.2	28.6
HBuf	48.5	36.3
Imp	66.4	54.1
Luminal membrane fluxes, $nmol/s\,cm^{-2}$		
Na^+	9.35	11.13
K^+	-0.42	-0.45
Cl^-	2.30	2.19
HCO_3^-	-0.99	-0.95
$HPO_4^=$	-0.03	-0.04
$H_2PO_4^-$	0.28	0.28
Glucose	1.97	1.85
Urea	0.01	0.01
HCO_2^-	-1.35	-1.28
H_2CO_2	1.10	1.07
NH_3	-0.03	-0.02
NH_4^+	-0.20	-0.23
H^+	-7.10	-8.93
Membrane flux components, $nmol/s\,cm^{-2}$		
Luminal membrane		
Na^+/H^+ (Na^+)	6.89	8.76
Na^+–Glucose	1.97	1.85
Na^+–$H_2PO_4^-$	0.28	0.28
Na^+–NH_4^+ (Na^+)	0.20	0.24
Cl^-/HCO_3^- (Cl^-)	0.95	0.90
Cl^-/HCO_2^- (Cl^-)	1.35	1.28
Lateral membrane		
K^+–Cl^-	1.28	1.57
Na^+–$3HCO_3^-$ (Na^+)	2.11	2.47
Na^+–$2HCO_3^-/Cl^-$ (Na^+)	0.97	0.58
Na^+, K–ATPase (Na^+)	8.26	9.24
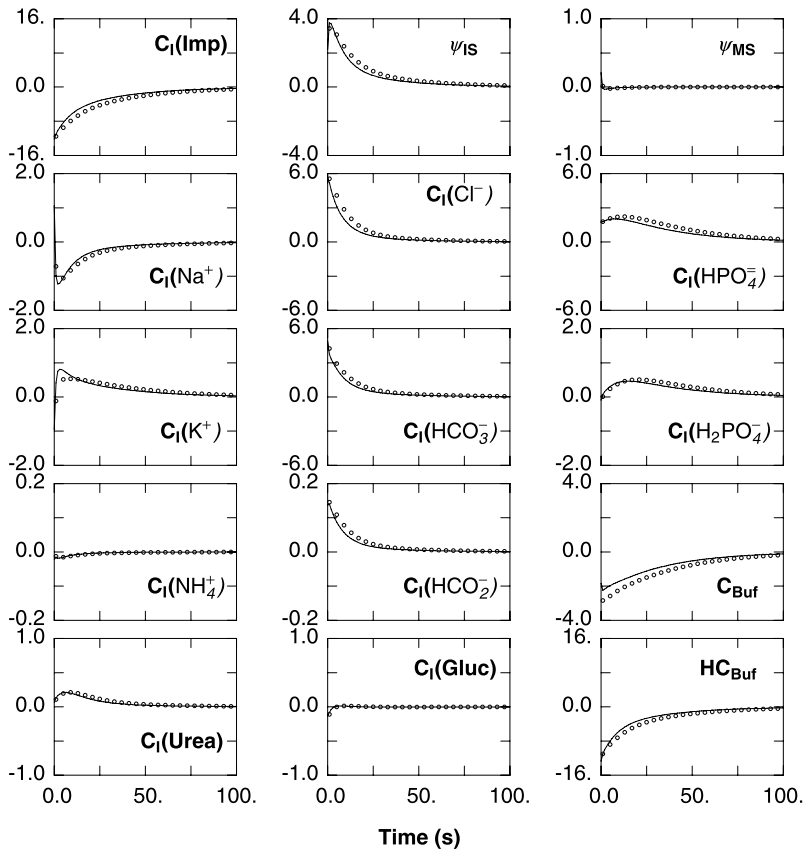
Fig. 3 Response to the perturbation of a 2-fold increase in Na^+/H^+ exchange activity. Lumen composition is that of mid-proximal tubule, low glucose and low HCO_3^-. The steady-state solution corresponding to doubling of Na^+/H^+ exchanger density is the initial point, u_0, and at $t = 0$, Na^+/H^+ density is returned to baseline. With the exception of the deflections in peritubular potential, ψ_{IS}, and transepithelial potential, ψ_{MS} (mV), ordinates are the concentration differences from baseline, of the important cytosolic components (mmol/l). Circles are the solution of the full model; the solid curves are generated by the linear dynamical system, starting at $x_0 = C^t u_0$, and mapped back into the u-coordinates by C.

from 4.0 to 2.0 nmol/s cm^2; with a slightly more acidotic cell and slightly lower cytosolic Na$^+$, flux through the Na$^+$/H$^+$ exchanger has increased from 6.5 to 7.1 nmol/s cm^2. The corresponding values in column 2 were obtained by increasing the density of the luminal Na$^+$/H$^+$ exchanger by 100%. Since turnover of the exchanger is equivalent to entry of NaHCO$_3$, this perturbation increases cytosolic HCO$_3^-$ (21%) and Na$^+$ (6%), as well as cell volume (23%). This doubling of Na$^+$/H$^+$ exchanger density yields only a 26% increase in flux through the transporter, due to the inhibitory effects of the changes in cytosolic composition, and the overall increase in luminal Na$^+$ entry is smaller (19%), due to blunting of other entry pathways. These changes are comparable to those observed with the early proximal fluid (Weinstein, 2004).

Table 2 Optimized dynamical system recovery times (42) from a 2-fold increase in Na^+/H^+ activity

Model conditions for early proximal tubule cell

Optimization criterion	Cost variable		
	$J_{MI}(Na^+)$	Cell volume	$C_I(HCO_3^-)$
Baseline	2.574	8.576	3.886
Cell volume	6.870	0.723	6.561
$C_I(HCO_3^-)$	0.175	5.672	0.675
$J_{MI}(Na^+)$	0.388	6.006	1.203
$Vol + C_I(HCO_3^-) + J_{MI}(Na^+)$	0.901	0.908	0.677

Model conditions for mid-proximal tubule cell

Optimization criterion	Cost variable		
	$J_{MI}(Na^+)$	Cell volume	$C_I(HCO_3^-)$
Baseline	2.192	8.230	3.653
Cell volume	9.429	1.298	8.561
$C_I(HCO_3^-)$	0.148	6.257	0.476
$J_{MI}(Na^+)$	0.257	6.516	0.873
$Vol + C_I(HCO_3^-) + J_{MI}(Na^+)$	0.835	1.653	0.344

The steady-state solution corresponding to the doubling of Na^+/H^+ exchanger density has been used as an initial perturbation, u_0, and the time-dependent model equations (with Na^+/H^+ density returned to its control value) predict the recovery to baseline. Denoting $u(t)$, the difference between the 31 model variables and their baseline values, 15 of these variables are displayed in Fig. 3, as the small circles. For each panel, the abcissa is time, and with the exception of the peritubular potential (ψ_{IS}) and transepithelial potential (ψ_{MS}), the ordinates are the concentration differences (relative to control) of the important cytosolic components (mmol/l); the cytosolic impermeant (Imp) is the model variable used to track cell volume. The remaining variables are cell NH_3 and H_2CO_2 concentrations, along with conditions in the lateral intercellular space. All of these are relatively constant, and of little interest. When the linearization process is applied to the model at the mid-proximal condition, one generates the 9×9 system matrix, A, and the isometry, C, mapping the coordinates of the reduced system, x, to u. The plot of $Cx(t)$ is displayed in Fig. 3 as the solid curves. To enhance the comparison between the linearization and the model, it must be acknowledged that the initial perturbation used in the calculations of the full system is not exactly that shown in Table 1, but corresponds to the projection CC^t of those values onto the tangent plane at the reference point. The difference between u_0 and $CC^t u_0$ is not large (about 0.05% the length of u_0). As indicated in the previous section, Na^+ flux across the luminal membrane can be estimated in the linearized model by the derivative m_{JNa} (30), and this derivative is different from early proximal to mid-proximal conditions. Figure 4 contains plots of luminal Na^+ flux during recovery from the doubling of Na^+/H^+ transporter density in both conditions. Small circles are values calculated from the full model, and solid curves are estimates from their linearizations. The concordance seems to be sufficient to allow these estimated fluxes to be used in formulating the cost function for optimization.

For the optimization problem, there are costs associated with the perturbation of model parameters and costs associated with the trajectory points. As indicated in the previous
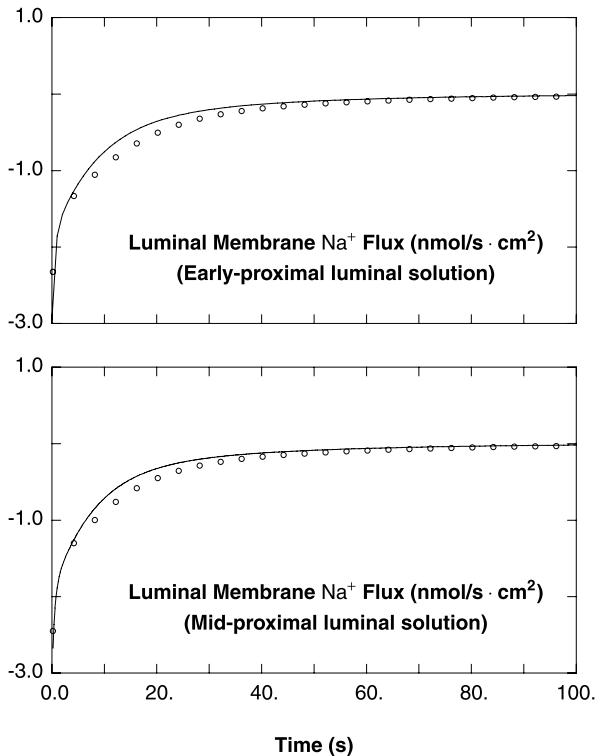
Fig. 4 Luminal membrane Na^+ fluxes during recovery from a 2-fold increase in Na^+/H^+ exchange activity. For the calculations of Fig. 3, the luminal membrane Na^+ flux is shown as its deviation from baseline. Circles are the solution of the full model; the solid curves are generated by the linear dynamical system with the estimate derived from (30) $\Delta J_{MI}(Na^+) = m_{JNa}Cx(t)$.

section, the parameter cost given by the matrix K, has been taken as the sum of the squares of the 24 fractional parameter changes, all scaled by a common factor, k (in this case $k = 5 \times 10^{-5}$). In the prior work (Weinstein, 2004), the trajectory costs were either the norm of the point (the same for either x or $u = Cx$), or the absolute value of the perturbation of the cellular impermeant (i.e. the fourth component of Cx). In the problems displayed in Fig. 5, the trajectory costs correspond to either the cellular impermeant, the cellular HCO_3^- concentration, or the luminal cell membrane Na^+ flux. For each of these trajectory costs, an algebraic Riccati equation is solved for optimal state feedback, F, and the dynamical systems incorporating this feedback control are identified (system matrix $A + BF$). Then using the initial perturbation of Figs. 3 and 4, (the steady-state solution to a doubling of luminal Na^+/H^+ exchanger density), the system relaxes back to the reference state. As in Figs. 3 and 4, the luminal conditions used in Fig. 5 correspond to mid-proximal tubule. What is displayed in Fig. 5 are four variables derived from $x(t)$: rows 1, 2, and 4 are just components of $u(t) = Cx(t)$, namely perturbations of peritubular cell membrane electrical potential, cytosolic impermeant, and cytosolic HCO_3^-; the panels of row 3 are the estimate of luminal membrane Na^+ flux, $m_{JNa}u(t)$. The left panels correspond to cell

Table 3 SubMatrix of the optimal feedback controller

3a. Model conditions for early proximal tubule cell

Transporter	Cost variable								
	Volume			$C_I(HCO_3^-)$			$J_{MI}(Na^+)$		
	ψ_{IS}	P_E	$C_I(lmp)$	ψ_{IS}	P_E	$C_I(lmp)$	ψ_{IS}	P_E	$C_I(lmp)$
$H_{MI}(K^+)$	−0.311	0.019	−0.392	−0.199	0.029	−0.008	−0.111	0.026	−0.006
$H_{MI}(Urea)$	0.000	0.000	0.001	−0.000	0.000	0.000	−0.000	0.000	0.000
$H_{MI}(H_2CO_2)$	0.028	0.010	0.087	−0.236	0.056	0.006	−0.053	0.019	0.001
$H_{MI}(NH_3)$	0.000	−0.000	0.000	0.001	−0.000	−0.000	−0.001	0.000	0.000
$H_{MI}(NH_4^+)$	0.004	−0.000	0.003	−0.001	0.000	0.000	−0.001	0.001	0.000
Cl^-/HCO_3^-	0.048	0.017	0.153	−0.337	0.080	0.009	−0.063	0.024	0.002
Cl^-/HCO_2^-	0.019	0.008	0.065	−0.078	0.018	0.003	−0.002	0.002	0.001
$Na^+/H_2PO_4^-$	−0.097	0.043	0.154	−0.225	0.047	0.002	−0.031	0.006	−0.001
$Na^+/Gluc$	2.714	−0.234	2.891	0.136	0.054	0.060	1.177	−0.326	0.036
Na^+/H^+	0.602	0.077	1.238	2.820	−0.632	−0.023	1.567	−0.484	0.024
$H_{IS}(K^+)$	−1.043	−0.185	−1.999	−5.327	1.116	−0.005	−3.426	1.050	−0.060
$H_{IS}(HPO_4^=)$	0.044	−0.010	−0.021	0.202	−0.043	−0.001	0.059	−0.017	0.001
$H_{IS}(H_2PO_4^-)$	0.071	−0.024	−0.074	0.304	−0.065	−0.003	0.046	−0.011	0.001
$H_{IS}(Gluc)$	0.238	−0.053	0.114	1.376	−0.308	−0.017	0.683	−0.220	0.005
$H_{IS}(Urea)$	−0.000	−0.000	−0.001	0.001	−0.000	−0.000	0.001	−0.000	0.000
$H_{IS}(HCO_2^-)$	0.002	−0.000	0.001	0.008	−0.002	−0.000	0.004	−0.001	0.000
$H_{IS}(H_2CO_2)$	−0.000	0.004	0.019	0.035	−0.008	−0.000	0.031	−0.010	0.001
$H_{IS}(NH_3)$	−0.004	−0.000	−0.006	−0.005	0.001	−0.000	−0.009	0.003	−0.000
$H_{IS}(NH_4^+)$	0.006	0.000	0.008	0.019	−0.004	0.000	0.016	−0.005	0.000
$K^+–Cl^-$	−0.065	−0.083	−0.510	0.106	−0.038	−0.017	−0.005	−0.013	−0.009
$Na^+–3HCO_3^-$	0.781	−0.029	0.606	4.320	−0.938	−0.030	2.586	−0.816	0.029
$Na^+–2HCO_3^-/Cl^-$	−0.010	0.001	−0.013	0.028	−0.006	0.000	0.031	−0.011	0.000
$Na^+, K^+–ATPase$	0.157	−0.008	0.405	−0.031	0.007	0.001	0.332	−0.113	0.002
$H^+–ATPase$	−0.277	0.041	−0.232	0.198	−0.057	−0.010	−0.018	0.001	−0.003

impermeant as the cost; central panels to cell HCO_3^-; and right panels to a cost for Na^+ flux. In each panel the solid curves are the result of optimal state control, and the dashed curves show the uncontrolled relaxation. It should be clear that for each of the controllers, the respective optimal controller brings it promptly back to the reference point, but this can be at the expense of other variables. In particular, for impermeant (cell volume) control, there are wide swings in Na^+ flux, in electrical potential, and in cytosolic HCO_3. Of note, the control of either HCO_3^- or Na^+ flux provides enhanced recovery of the other variable, along with enhanced recovery of cell potential. Neither controller provides very much improvement in the recovery of cell volume. Recovery times for a specific trajectory cost may be quantified as $\tau(x_0)$:

$$\tau(x_0) = \frac{2}{(x_0, N x_0)} \int_0^\infty \big(x(t), N x(t)\big)\, dt, \tag{42}$$

in which the matrix N is the cost referred to the dynamical system (29). In Table 2, the integrals (42) have been determined numerically to 100 s for each of the three costs under consideration. They are shown for the problems of Fig. 5, and for the same problems

Table 3 (*Continued*)

3b. Model conditions for mid-proximal tubule cell

Transporter	Cost variable								
	Volume			$C_I(HCO_3^-)$			$J_{MI}(Na^+)$		
	ψ_{IS}	P_E	$C_I(lmp)$	ψ_{IS}	P_E	$C_I(lmp)$	ψ_{IS}	P_E	$C_I(lmp)$
$H_{MI}(K^+)$	−0.181	−0.007	−0.353	−0.209	0.047	−0.003	−0.109	0.036	−0.003
$H_{MI}(Urea)$	0.000	0.000	0.002	−0.000	0.000	0.000	−0.000	0.000	0.000
$H_{MI}(H_2CO_2)$	0.054	0.026	0.205	−0.307	0.084	0.010	−0.090	0.038	0.002
$H_{MI}(NH_3)$	−0.002	−0.000	−0.003	−0.006	0.002	0.000	0.006	−0.003	−0.000
$H_{MI}(NH_4^+)$	0.003	−0.000	0.003	0.001	−0.000	0.000	−0.001	0.000	0.000
Cl^-/HCO_3^-	0.073	0.040	0.298	−0.337	0.091	0.012	−0.080	0.035	0.003
Cl^-/HCO_2^-	0.038	0.024	0.172	−0.103	0.027	0.004	−0.003	0.003	0.002
$Na^+/H_2PO_4^-$	−0.168	0.092	0.308	−0.204	0.050	0.002	−0.025	0.006	−0.001
$Na^+/Gluc$	1.068	−0.041	1.554	0.515	−0.112	0.012	0.761	−0.271	0.012
Na^+/H^+	0.651	0.188	1.904	2.270	−0.590	−0.031	1.656	−0.609	0.016
$H_{IS}(K^+)$	−0.830	−0.326	−2.426	−5.029	1.270	0.047	−3.742	1.387	−0.033
$H_{IS}(HPO_4^=)$	0.073	−0.021	−0.036	0.215	−0.054	−0.003	0.087	−0.031	0.001
$H_{IS}(H_2PO_4^-)$	0.138	−0.053	−0.133	0.306	−0.076	−0.004	0.062	−0.019	0.001
$H_{IS}(Gluc)$	0.118	−0.028	0.077	0.646	−0.168	−0.012	0.407	−0.155	0.001
$H_{IS}(Urea)$	−0.000	−0.000	−0.002	0.001	−0.000	−0.000	0.001	−0.000	−0.000
$H_{IS}(HCO_2^-)$	0.003	−0.000	0.003	0.014	−0.003	−0.000	0.010	−0.004	0.000
$H_{IS}(H_2CO_2)$	−0.008	0.005	0.012	0.033	−0.009	−0.001	0.027	−0.010	0.000
$H_{IS}(NH_3)$	0.002	0.001	0.006	0.008	−0.002	−0.000	0.010	−0.004	0.000
$H_{IS}(NH_4^+)$	0.006	0.001	0.012	0.029	−0.008	−0.000	0.026	−0.010	0.000
$K^+–Cl^-$	−0.071	−0.145	−0.807	0.126	−0.042	−0.016	0.026	−0.022	−0.008
$Na^+–3HCO_3^-$	0.919	−0.010	0.894	5.335	−1.369	−0.080	3.797	−1.428	0.018
$Na^+–2HCO_3^-/Cl^-$	−0.051	0.001	−0.080	0.161	−0.042	−0.003	0.117	−0.046	−0.000
$Na^+, K^+–ATPase$	−0.057	0.050	0.388	−0.042	0.009	−0.000	0.273	−0.110	−0.001
$H^+–ATPase$	−0.108	0.017	−0.110	0.011	−0.007	−0.003	−0.033	0.011	−0.001

using early proximal tubule fluid. This simply quantifies the observations made in examination of the figure. What is also shown in Table 2 are recovery times obtained when the optimal control problem is solved for a cost matrix that is the sum of matrices of the three elementary problems. For that controller, there is improvement in all three costs. (It may be noted in Table 2 that the smallest recovery time for $J_{MI}(Na^+)$ actually occurs in the optimization for $C_I(HCO_3^-)$. What is being minimized in these problems is the integral of $(x, N + F^t K F x)$, in (32), namely a trajectory cost (N) plus a parameter cost ($F^t K F$). In Table 2, only costs from the trajectory component of the cost function, (42), are shown.)

With the intention to translate optimal control of the dynamical system to cellular homeostasis in the full proximal tubule cell model, it is important to examine the feedback matrix solutions of the Riccati equations. This is most fruitfully done in terms of the physiologic variables, so that the matrix of interest is FC^t, a 24×31 array. With respect to the calculations of Fig. 5 and Table 2, there are six such matrices, corresponding to early and mid-proximal luminal solutions, and to cost functions based on cell volume, cell HCO_3^-, or luminal Na^+ flux. For this to be meaningful, each of these matrices is normalized, the row entries by p_{ss} and the column entries by u_0, the reference parameters and system variables (i.e. in place of $FC^t(i, j)$, $FC^t(i, j) \cdot u_0/p_{ss}(i)$ is displayed).
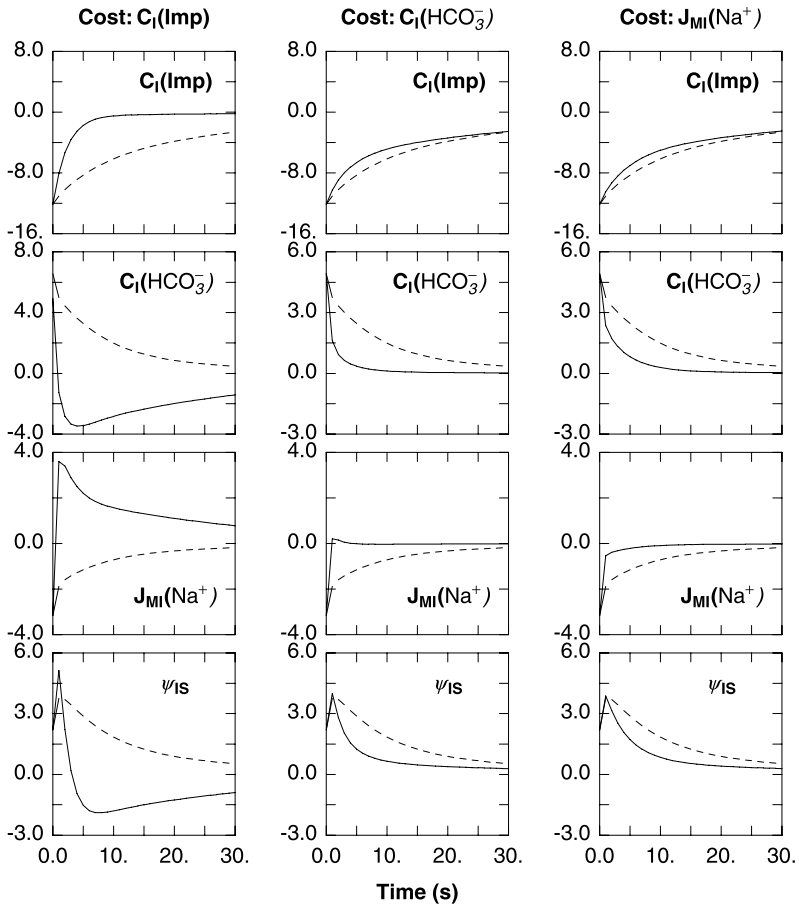
Fig. 5 Recovery trajectories in the dynamical system with optimal control. Initial conditions are those of Figs. 3 and 4, using mid-proximal luminal solution and the perturbation given by a 2-fold increase in Na^+/H^+ activity. In each column of panels, predicted luminal Na^+ flux (nmol/s cm^2), peritubular membrane electrical potential (mV), cellular impermeant (mmol/l), and cell HCO_3^- (mmol/l), are displayed during recovery to baseline. Trajectory costs for the Ricatti equation correspond to the deviation from reference of the cellular impermeant (left column), the cell HCO_3^- concentration (center column), or the luminal cell membrane Na^+ flux (right column). In each panel solid curves are the result of optimal state control, and dashed curves show uncontrolled relaxation.

The resulting array displays fractional changes in the model parameters as a function of fractional changes in the system variables. When this is done, most of the entries of most of the columns are close to zero. Specifically, none of the optimal control solutions relies upon control by cytosolic Na^+ or HCO_3^- concentrations. The only substantial entries are in the columns corresponding to cellular electrical potential, cellular impermeant concentration, and the hydrostatic pressure of the lateral intercellular space; for the six problems, these columns are shown in Table 3. The first observation is that when cell volume provides the trajectory cost, then cell volume plays the most important role in

feedback control. For both early and mid-proximal solutions, the most important luminal control is that of the Na^+–glucose cotransporter and the Na^+/H^+ exchanger. (Positive dependence on the cytosolic impermeant implies that both of these transporters are activated by decreases in cell volume.) For the mid-proximal solution, with its lower glucose concentration, reliance on the Na^+–glucose cotransporter is diminished. When volume provides the trajectory cost, important peritubular membrane controllers are the K^+ channel and K^+–Cl^- cotransporter, which show a strong positive dependence on cell volume, and the peritubular Na^+–$3HCO_3^-$ cotransporter, which is activated with cell shrinkage. The impact each solute transporter (model parameter) on the cell physiology (state variables) can be discerned from the steady-state formulation of (21). This is embodied in the matrix, $R^{-1}Q = \frac{du}{dp}$, and a portion of this 31×24 matrix is displayed in Table 4 (with rows normalized by u_0 and columns by p_0, to display fractional dependence). With reference to Table 4, activation of the peritubular K^+ channel and K^+–Cl^- cotransporter can be expected to increase the cell impermeant (decreasing cell volume), while inactivation of the Na^+–$3HCO_3^-$ cotransporter would blunt this effect. One rationalization of the decrease in Na^+–$3HCO_3^-$ activity is that this decrease acts to limit the depletion of cell HCO_3. Both the K^+ channel and the K^+–Cl^- cotransporter act to decrease cytosolic HCO_3^- (Table 4 and Fig. 5), and a decrease in cell HCO_3^- activates luminal Na^+/H^+ exchange (Weinstein, 1995), a potent force for increasing cell volume.

When the trajectory costs are either deviations in cytosolic HCO_3^- concentration or luminal Na^+ flux, the important controllers are the cellular electrical potential, ψ_{IS}, and to a lesser extent, the lateral interspace hydrostatic pressure; there is virtually no role for volume-dependent transporters in this homeostatic response. It should be noted that in both Tables 3 and 4, the fractional changes in cell potential are determined by dividing by the reference potential of approximately -60 mV, so that "hyperpolarizing" displacements (more electronegative) correspond to positive entries. With the doubling of Na^+/H^+ activity, the cell is alkalinized, depolarized, and shows an increase in interspace hydrostatic pressure (Table 1). With reference to the optimal control matrices in Table 3a and 3b, both the depolarization and the interspace pressure are expected to increase the activity of the peritubular K^+ channel and decrease the activity of luminal Na^+/H^+ exchange and glucose cotransport. With reference to Table 4, all three of these transport effects are expected to decrease the cytosolic HCO_3^-. Inhibition of the Na^+–$3HCO_3^-$ cotransporter is also expected, but this would tend to counteract the impact of the other transporters on cell HCO_3^-. By virtue of the Na^+, K^+–ATPase, transcellular Na^+ flux tends to be proportional to cell Na^+ concentration, so the impact of a transporter on cell Na^+ (Table 4) can serve as a surrogate for its effect on Na^+ flux. The decrease in activity of luminal membrane Na^+/H^+ and Na^+–glucose cotransport, are intuitively clear, and both act to restore increased Na^+ flux to normal. Inhibition of the peritubular Na^+–$3HCO_3^-$ cotransporter also acts to decrease cell Na^+, but the mechanism is likely indirect. When this transporter alkalinizes the cell, there is a strong pH-inhibition of the luminal Na^+/H^+ exchanger (Weinstein, 1995). Counter to the restorative impact of the other three transporters, increased activity of the peritubular K^+ channel can be expected to increase Na^+ flux.

The concerted action of feedback control to simultaneously restore cell volume and HCO_3^- concentration, along with luminal Na^+ flux, is achieved by summing the three cost matrices, and solving the appropriate Riccati equation. The results for early and mid-proximal solutions are displayed in the left columns of Figs. 6a and 6b (solid curves), along with the uncontrolled relaxation (dashed curves). The improvement is clear, and

Table 4 Impact of membrane transporters on cell composition and electrical PD: fractional change in state variables relative to fractional parameter change

	$H_{MI}(K^+)$	Cl^-/HCO_3^-	Na^+-Gluc	Na^+/H^+	$H_{IS}(K^+)$	K^+-Cl^-	$Na^+-3HCO_3^-$	$Na^+,K^+-ATPase$
ψ_{IS}	0.0292	−0.0058	−0.0598	−0.0492	0.2166	0.0449	−0.1129	−0.0063
$C_I(Imp)$	0.0218	−0.0399	−0.0371	−0.2369	0.1385	0.1411	0.1842	−0.1349
$C_I(Na^+)$	0.0146	0.0192	0.0583	0.0914	0.0975	0.0488	0.0861	−0.4878
$C_I(K^+)$	−0.0026	−0.0058	−0.0217	−0.0060	−0.0171	−0.0024	−0.0042	0.0640
$C_I(Cl^-)$	−0.0339	0.1890	0.0738	0.4649	−0.1846	−0.3526	−0.3538	−0.0869
$C_I(HCO_3^-)$	−0.0211	0.0102	0.0054	0.2901	−0.1371	−0.1158	−0.2025	0.1726
$C_I(Gluc)$	0.0155	−0.0074	0.3371	−0.0655	0.1022	0.0098	−0.1014	0.1306

has been quantified in the recovery times of Table 2. One problem with importing state control into the full model of the proximal tubule cell, is that certain controllers are not "physiologic", in that they have never been identified as such by experimentalists. This applies especially to the lateral interspace hydrostatic pressure (although see discussion below). In the prior work (Weinstein, 2004), only four (of the 31 physiologic variables) were considered admissible as control signals: cell volume, cytosolic Na^+ and HCO_3^- concentrations, and cell membrane electrical potential. In that work, only those 4 columns of the feedback matrix, FC^t, were incorporated into the full proximal tubule cell model, and recovery times (for total displacement or for cell volume) appeared to improve. It is possible to ask, in the context of the approximate dynamical system, whether this approach can be expected to work. To address this question, we denote the projection, W, of the physiologic vector u onto its 4 "admissible" components, and consider the dynamical system with control

$$x' = Ax + Bp = (A + BFC^t WC)x. \tag{43}$$

With the matrix, F, the optimal controller identified for the combined costs of volume, HCO_3^-, and $J_{MI}(Na^+)$, the system (43) is integrated and displayed in the right-hand columns of Figs. 6a and 6b (solid curves), along with the uncontrolled relaxation. It is clear that for the early proximal fluid, recovery using only the "physiologic variables" is nearly as good as that with full state control (left panel). For the mid-proximal solution, recovery with the truncated set of variables does appear to be more prompt, but there are substantially wider swings in the model variables.

   To export the controller identified by the dynamical system to the full proximal tubule model, parameter increments, $p(t)$, are computed in terms of the deviations of the physiologic variables, $u(t)$

$$p(t) = FC^t Wu(t) \tag{44}$$

and incorporated into the model calculations at each time step. For the calculations of Fig. 7, the initial condition is the steady state computed with reference parameters, except for a doubling of luminal Na^+/H^+ exchanger density. At $t = 0$, there is then a step change to baseline Na^+/H^+ level, and feedback control is included. The figure displays relaxation to reference, with early tubule and mid-tubule luminal fluid concentrations in left- and right-side panels. In each panel, solid curves are computed by the model with control (44), and the dashed curves are the model with reference parameters. Of note, the initial cell volumes and cell HCO_3^- concentrations are identical between controlled and reference models, as required by the identical initial conditions. There is, however, a discrepancy at $t = 0$ between the two models, with respect to the cell electrical potential and Na^+ flux. This is due to the fact that fluxes and electrical potential will be affected by the different transporter permeabilities computed in the model with parameter control. Improvement in recovery rates provided by feedback control is evident in the graphs of electrical potential, cell volume and cell HCO_3^-. It is less obvious in the plot of luminal Na^+ flux (upper panels), but when the recovery times are quantified according to (42) and summarized in Table 5, the improvement is documented. Table 5 also includes results from a set of calculations in which feedback control is increased by solving the Riccati equations with a cheaper cost for parameter control ($k = 5 \times 10^{-6}$, a 90% reduction). In this case the
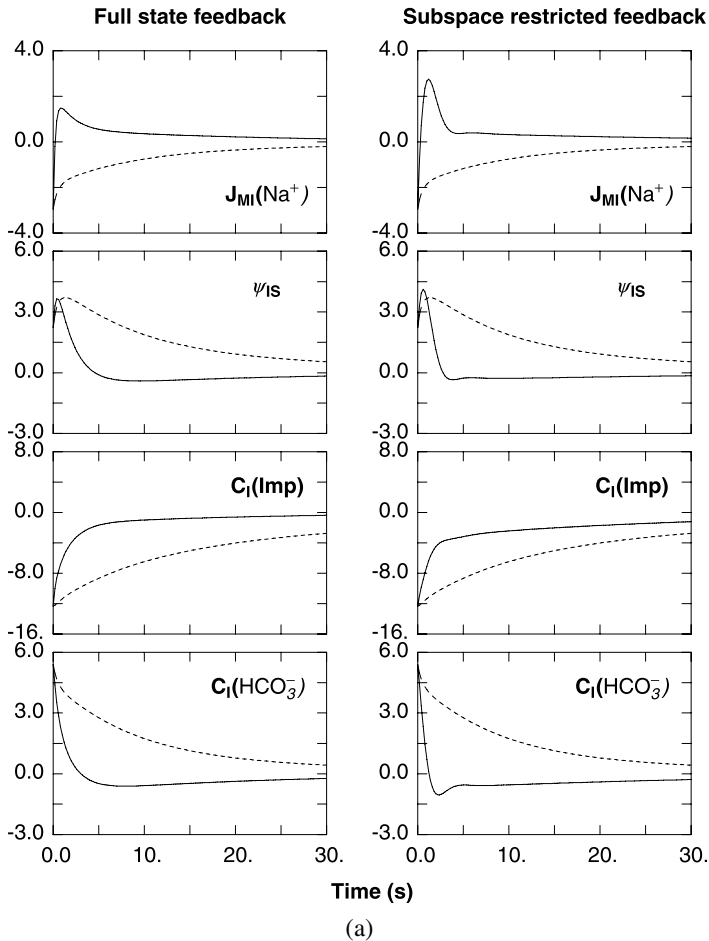
Fig. 6 (a) Recovery trajectories in the dynamical system with optimal control restricted to a sub-space. Model conditions are early luminal solution, and the initial perturbation is given by a 2-fold increase in Na^+/H^+ activity. In each column of panels, predicted luminal Na^+ flux (nmol/s cm^2), peritubular membrane electrical potential (mV), cellular impermeant (mmol/l), and cell HCO_3^- (mmol/l), are displayed during recovery to baseline. In the left panels, trajectory costs for the Ricatti equation correspond to the sum of the deviations from reference of the cellular impermeant plus the cell HCO_3^- concentration plus the luminal cell membrane Na^+ flux. Solid curves are the result of optimal state control, and dashed curves show uncontrolled relaxation. In the right panels, feedback control has been restricted to a subspace spanned by the cell impermeant, peritubular membrane electrical potential, and concentrations of Na^+ and HCO_3^-.

parameter sensitivities are roughly 5-fold greater than those used for Fig. 7, and there is additional improvement for most of the recovery times.

The premise of glomerulotubular balance is that proximal epithelial Na^+ reabsorption is proportional to axial fluid flow along the tubule. Thus, rather than cellular recovery from a displacement, the natural problem to consider is that of cellular homeostasis in
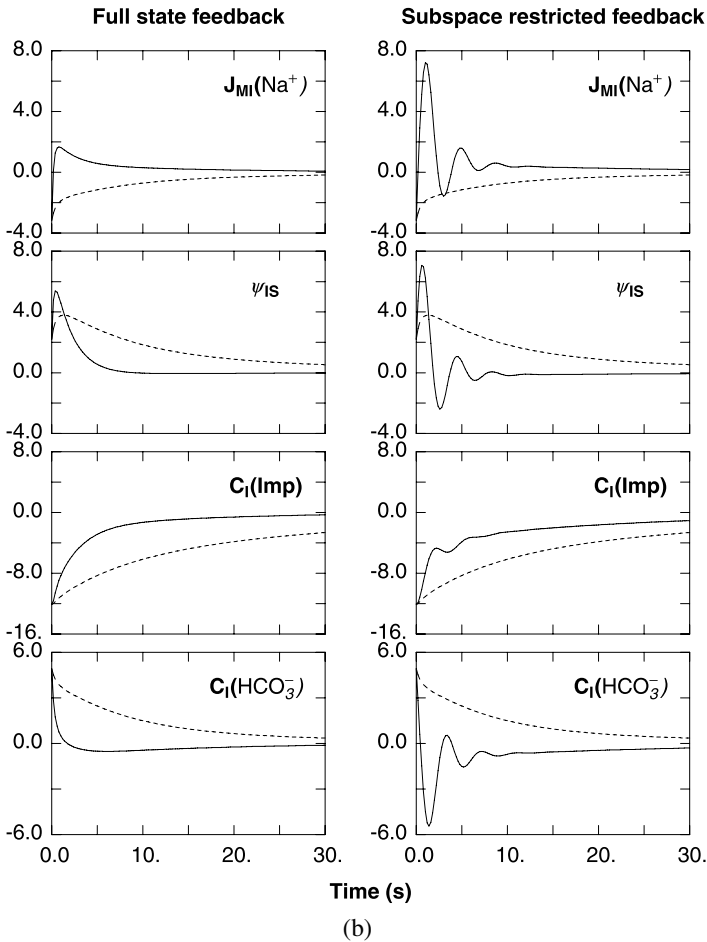
Fig. 6 (b) Recovery trajectories in the dynamical system with optimal control restricted to a subspace. Model conditions use the mid-proximal luminal solution, and are otherwise identical to those of Fig. 6a.

the face of variable throughput, and this consideration motivated attention to the tracking problem, displayed in (36)–(41). To start this problem, one first selects the signal to track, $r(t) = (0, 0, v(t))^t$, where $v(t)$ scales the increment in luminal membrane Na$^+$ flux. In the calculations below,

$$V(t) = \begin{cases} 16(t/50), & 0 \le t \le 50, \\ 16(2 - t/50), & 50 \le t \le 100, \end{cases} \tag{45}$$

selected to simulate an increase and then recovery of luminal fluid flow over a 100 s interval. Of note, in calculating the tracking error, $e(t) = M_r u(t) - r(t)$, the matrix M_r which holds the estimate of luminal Na$^+$ flux, needs to be computed for each of the problems under consideration (early and mid-proximal luminal solutions). The next step is
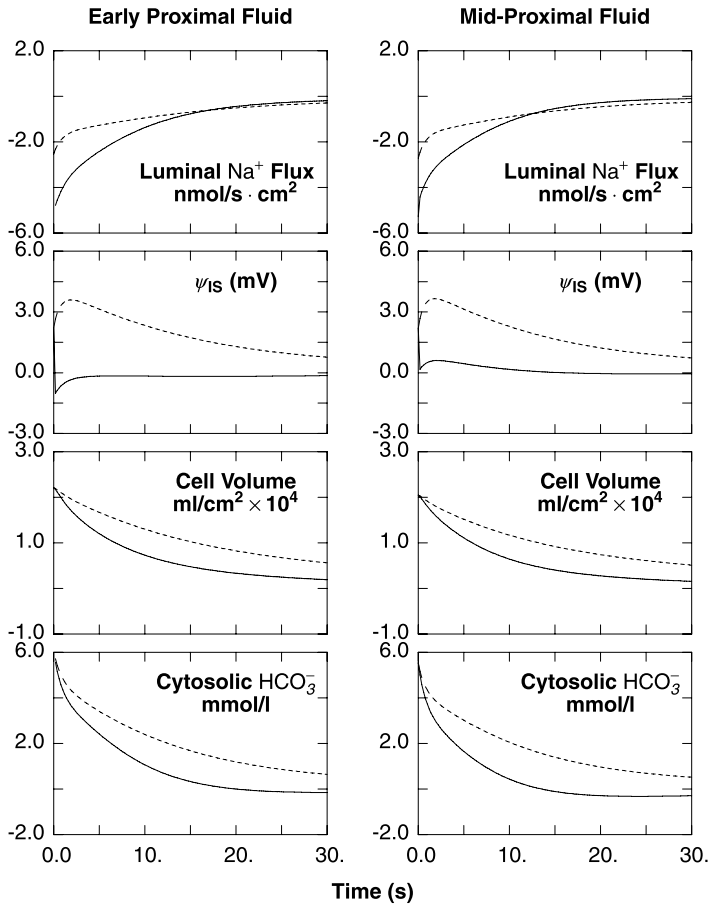
Fig. 7 Recovery trajectories in the full proximal tubule model with parameter control imported from the dynamical system. Columns on the left correspond to early luminal fluid and on the right to mid-proximal conditions. The initial condition is that of doubled Na^+/H^+ exchange, and the panels display relaxation to baseline of luminal Na^+ flux, peritubular membrane electrical potential, cellular impermeant, and cell HCO_3^-. Solid curves are obtained when parameter control is specified by the optimal feedback controller of Fig. 6, restricted to the subspace spanned by impermeant, peritubular membrane potential, and concentrations of Na^+ and HCO_3^-.

the solution of a final-value problem (39) for the auxiliary variable, $\beta(t)$, with $\beta(100) = 0$. To formulate this problem, the optimal feedback matrix F must be available from prior solution of the algebraic Riccati equation, in which the costs are precisely those utilized in the calculation of Fig. 6. Finally, the initial value problem (40) is solved for the trajectory, $x(t)$ (with $x_0 = 0$), and ultimately the model parameters, $p(t)$, from (41). Optimal model parameters consist of two terms, one the feedback $Fx(t)$, and the other, $-K^{-1}B^t\beta(t)$, an autonomous function of time which is computed prior to determination of the model trajectory. This autonomous parameter component can be incorporated directly into the full proximal tubule model.

Table 5 Recovery times from the full proximal tubule model: parameter control imported from the dynamical system to minimize aggregate cost Vol + $C_I(HCO_3^-)$ + $J_{MI}(Na^+)$

Model conditions for early proximal tubule cell

Optimization criterion	Cost variable		
	$J_{MI}(Na^+)$	Cell volume	$C_I(HCO_3^-)$
Baseline	4.225	10.239	4.842
Optimal control	2.025	4.489	2.344
Decreased parameter cost	0.793	2.256	2.598

Model conditions for mid-proximal tubule cell

Optimization criterion	Cost variable		
	$J_{MI}(Na^+)$	Cell volume	$C_I(HCO_3^-)$
Baseline	3.542	9.841	4.449
Optimal control	2.357	4.342	1.775
Decreased parameter cost	1.240	1.723	1.132

To export the solution of the tracking problem to the full proximal tubule model, the modified optimal controller (44) is used for the feedback, while the autonomous term is unaltered. With these rules for parameter modulation, the full model has been solved over the time interval (0, 100 s) with the initial condition being the reference state ($u(0) = 0$). Solutions for both early and mid-proximal conditions have been obtained, and several key variables are displayed in Fig. 8: luminal membrane Na^+ flux in the upper panels, and cell electrical potential, volume, and HCO_3^- in the lower three panels. The most important observation is that with either luminal composition, there is substantial change in $J_{MI}(Na^+)$: from 8.5 to 22.6 nmol/s cm^2 with early conditions, and 8.7 to 18.3 nmol/s cm^2 with mid-proximal conditions, and that these flux variations occur with relatively trivial changes in cell volume and HCO_3^-. This is precisely what was requested from the tracking problem for the dynamical system. Of the model variables that were considered "permissible" for feedback parameter modulation, cell membrane electrical potential is depolarized (negative excursion) and cell volume decreases (positive excursion for the cell impermeant). From the full proximal tubule model solutions, nine of the most important parameters have been displayed in Figs. 9a and 9b, as fractional changes from reference. Each panel contains three curves, the autonomous component input from the dynamical system, the feedback component computed at each time step, and the sum of these two increments. Table 6 displays the magnitudes of the fractional parameter changes at the midpoint, $t = 50$ s. One salient feature of this complex system is that the autonomous parameter changes are of opposite sign and dominate the feedback component, reflecting the fact that the cell is trying to establish an increasing Na^+ flux, not return to the reference state. It is important to acknowledge that some of the parameter components, autonomous and feedback, are at times large and negative. Since these parameters are all permeabilities, such contributions make no physical sense. However, in all cases that the sums (i.e. total parameter deviations) have magnitude greater than one, their signs are positive, and represent parameter increases.

For either luminal condition, the largest of the autonomous parameter variations are increases in the peritubular Na^+–$3HCO_3^-$ cotransporter. By itself, this will tend to increase $J_{MI}(Na^+)$ while shrinking and depolarizing the cell (Table 4). The autonomous increases
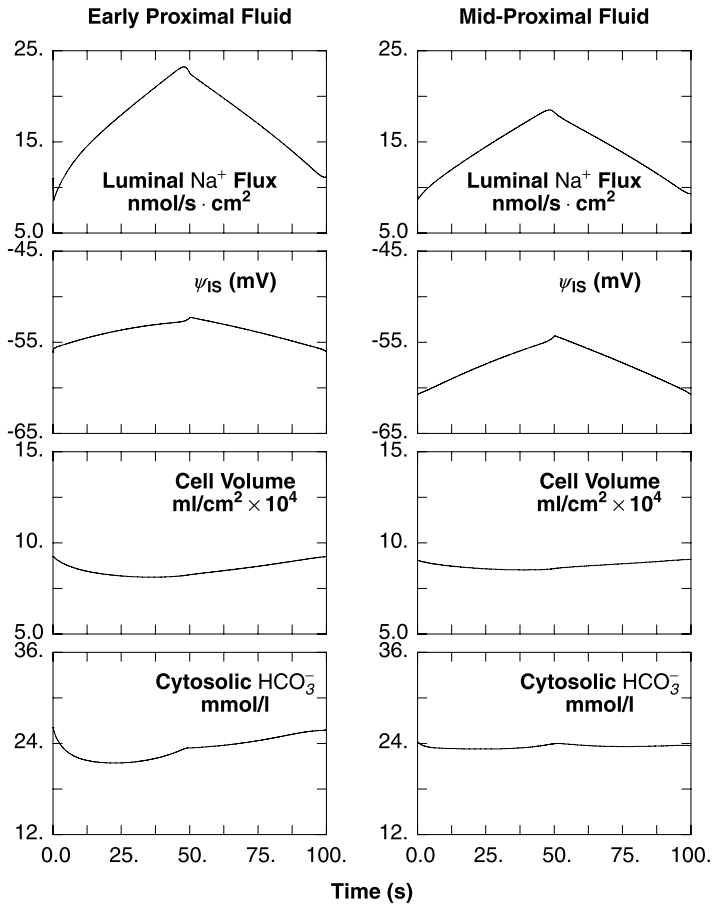
Fig. 8 Trajectories of a tracking problem in the full proximal tubule model, with parameter control imported from the dynamical system. The problem is to have luminal Na^+ flux increase and decrease approximately two-fold, with negligible disturbance of cell volume and HCO_3^-. Columns on the left correspond to early luminal fluid, and on the right to mid-proximal conditions; the initial condition is the steady-state baseline. Solution of the tracking problem in the associated dynamical systems (to generate an optimal feedback matrix plus an autonomous change in model parameters) is imported into the full model. As in the calculations of Fig. 7, only four columns of the feedback matrix are used.

in the luminal Na^+/H^+ antiporter, and the peritubular Na^+, K^+–ATPase also increase $J_{MI}(Na^+)$, although tending to increase cell volume. For both conditions, the autonomous activation of the peritubular K^+–Cl^- cotransporter will act in concert with the increase in turnover of the Na^+, K^+–ATPase to jettison the additional K^+ burden, and decrease cell volume. For the early luminal condition, this decrease in cell volume activates the Na^+–glucose cotransporter, which further augments $J_{MI}(Na^+)$. One unanticipated observation, especially notable with mid-proximal conditions, is the autonomous decrease in peritubular K^+ channel permeability. This vitiates the feedback increase in peritubular K^+ permeability that came as a result of electrical depolarization, and acts to shift the
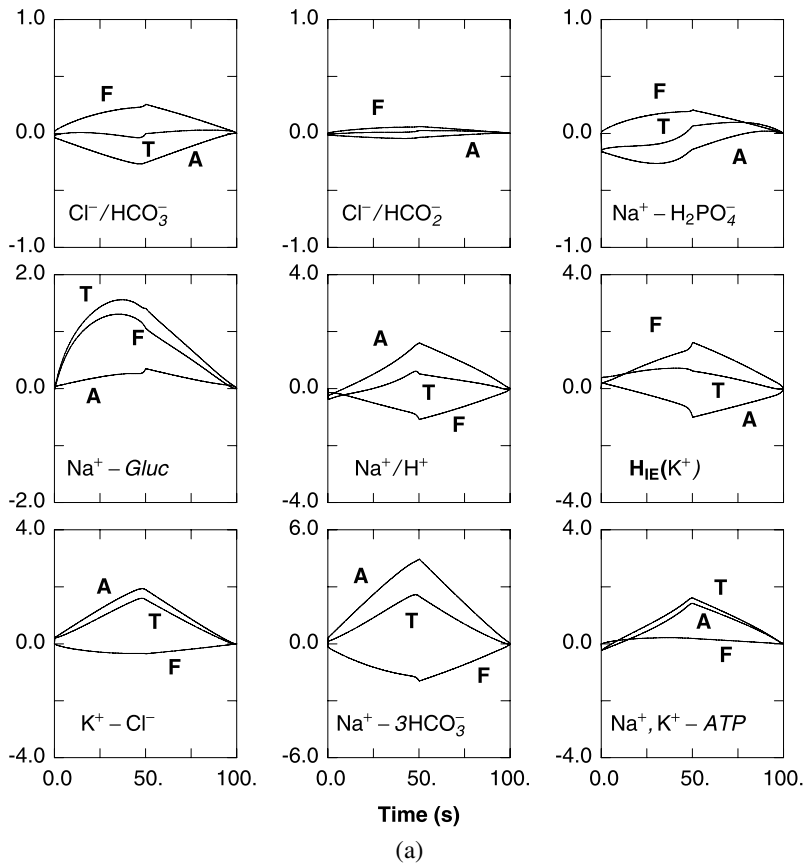
Fig. 9 (a) Parameter deviations during tracking in the full proximal tubule model. For the calculations of Fig. 8 (early luminal fluid), the fractional change (deviation relative to baseline) in 9 of the transporter densities are shown. The total deviation (T) is the sum of an autonomous term (A), imported directly from the dynamical system, plus a feedback term (F), computed from the reduced optimal feedback matrix and the trajectory point.

K^+ efflux to the K^+–Cl^- cotransporter. The overall role for the peritubular K^+ channel in tracking luminal flow changes is predicted to be small. Finally, it is necessary to examine the impact of these parameter changes on overall proximal epithelial function, with both cellular and paracellular pathways in parallel. If glomerulotubular balance is operative, there must be coordinate changes in tubular Cl^- reabsorption. Figure 10 displays the predicted fluxes of Na^+ (upper panels) and Cl^- (lower panels) for early and mid-proximal conditions. Each panel contains three curves, corresponding to predicted ion fluxes across the luminal cell membrane and across the tight junction, along with their sum. In the early proximal tubule, there is negligible tight junction Na^+ flux, due to opposing electro-diffusive and convective components. In contrast, tight junction Cl^- flux is substantially greater than that through the cell. The model predicts virtually no change
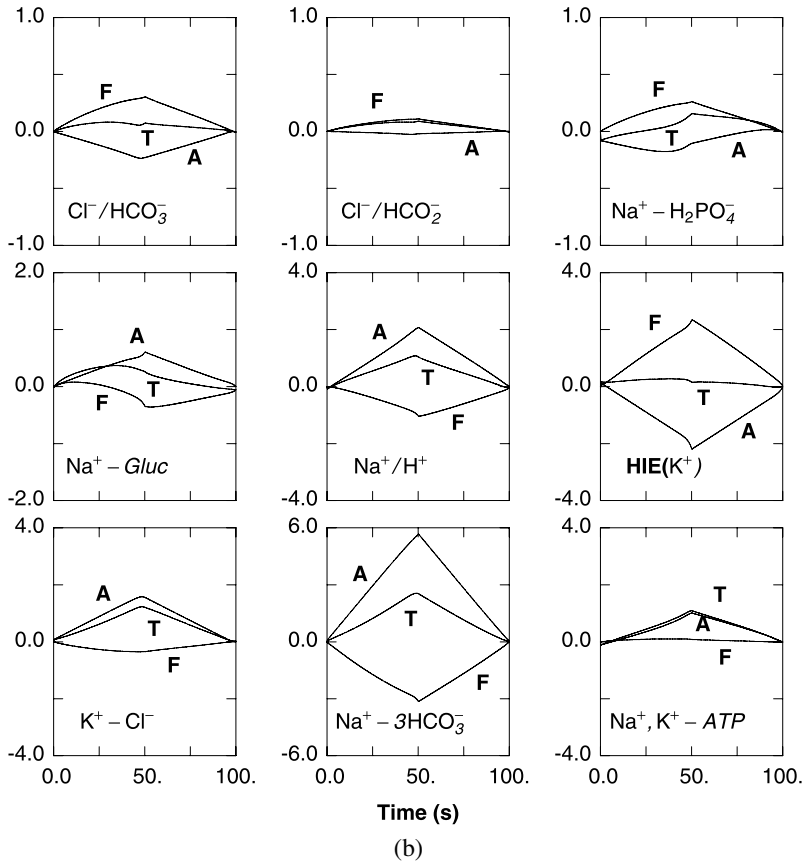
Fig. 9 (b) Parameter deviations during tracking in the full proximal tubule model. For the calculations of Fig. 8 (mid-proximal fluid), the fractional change (deviation relative to baseline) in 9 of the transporter densities are shown. The total deviation (T) is the sum of an autonomous term (A), imported directly from the dynamical system, plus a feedback term (F), computed from the reduced optimal feedback matrix and the trajectory point.

to the transcellular component of Cl^- flux, while the paracellular component tracks the variation in Na^+ flux, due to the luminal electronegativity deriving from Na^+–glucose cotransport, along with increases in tight junction convection. For the mid-proximal condition, there is a substantial component of tight junction Na^+ flux, due to the loss of luminal electronegativity (Table 1), but it shows little variation with the changing transcellular component. Both paracellular and transcellular components of Cl^- reabsorption are larger than in early proximal tubule, due to the decrease in mid-proximal HCO_3^-. (Lumen-to-blood Cl^- concentration gradient favors tight junction Cl^- reabsorption, and the more favorable cell-to-lumen HCO_3^- gradient favors cellular Cl^- uptake.) Again it is the tight junctional component of Cl^- flux that is predicted to vary, and this is due to changes in convective flow.

Table 6 Parameter control at $t = 50$ s for the full model tracking problem: fractional parameter deviation from baseline

	Early proximal tubule			Mid-proximal tubule		
	Total	Feedback	Autonomous	Total	Feedback	Autonomous
$H_{MI}(K^+)$	0.947	−0.095	1.041	0.807	0.125	0.682
$H_{MI}(Urea)$	−0.003	0.000	−0.003	−0.002	0.001	−0.003
$H_{MI}(H_2CO_2)$	−0.020	0.176	−0.196	0.011	0.261	−0.250
$H_{MI}(NH_3)$	−0.007	−0.001	−0.006	0.041	0.005	0.036
$H_{MI}(NH_4^+)$	−0.013	0.001	−0.014	−0.015	−0.002	−0.013
Cl^-/HCO_3^-	−0.004	0.253	−0.257	0.072	0.302	−0.230
Cl^-/HCO_2^-	0.025	0.060	−0.035	0.089	0.109	−0.020
$Na^+/H_2PO_4^-$	0.063	0.204	−0.141	0.154	0.260	−0.106
$Na^+/Gluc$	1.411	1.069	0.342	0.263	−0.338	0.601
Na^+/H^+	0.530	−1.064	1.595	1.044	−1.027	2.071
$H_{IS}(K^+)$	0.621	1.596	−0.975	0.157	2.323	−2.166
$H_{IS}(HPO_4^-)$	−0.143	−0.117	−0.026	−0.160	−0.161	0.001
$H_{IS}(H_2PO_4^-)$	−0.362	−0.201	−0.161	−0.439	−0.269	−0.170
$H_{IS}(Gluc)$	0.678	−0.713	1.391	0.177	−0.453	0.629
$H_{IS}(Urea)$	0.004	−0.001	0.005	0.003	−0.001	0.004
$H_{IS}(HCO_2^-)$	0.002	−0.003	0.005	0.003	−0.008	0.011
$H_{IS}(H_2CO_2)$	0.038	−0.010	0.047	0.032	−0.010	0.042
$H_{IS}(NH_3)$	−0.025	0.000	−0.026	0.020	−0.003	0.023
$H_{IS}(NH_4^+)$	0.025	−0.007	0.032	0.031	−0.014	0.045
K^+–Cl^-	1.555	−0.349	1.904	1.213	−0.349	1.562
Na^+–$3HCO_3^-$	2.514	−1.938	4.452	2.541	−3.119	5.660
Na^+–$2HCO_3^-/Cl^-$	0.059	−0.011	0.070	0.076	−0.095	0.171
Na^+, K^+–ATPase	1.609	0.188	1.421	1.094	0.085	1.009
H^+–ATPase	0.028	−0.217	0.246	0.150	0.022	0.128

5. Discussion

The calculations of this work begin with a mathematical model of rat proximal tubule that developed over several years, beginning with a basic representation of Na^+, K^+, Cl^-, HCO_3^- and phosphate transport across cellular and paracellular pathways (Weinstein, 1983), subsequently adding Na^+-coupled glucose transport (Weinstein, 1985), the powerful Cl^-/HCO_2^- exchanger at the luminal cell membrane (Weinstein, 1992), and ammonia, the predominant buffer for renal acid excretion (Weinstein, 1994). In view of its key role in proximal tubule Na^+ reabsorption, and the wealth of available kinetic data, a detailed kinetic model of the luminal membrane Na^+/H^+ (and Na^+/NH_4^+) exchanger later replaced the single-parameter nonequilibrium thermodynamic formulation (Weinstein, 1995). This marks the state of development of the proximal tubule model used in the calculations here. Despite the accrued detail, however, the model epithelium has remained remarkably linear in a physiologically meaningful neighborhood of its parameter space. This linearity had been exploited in a steady-state study of homeostatic parameter coordination (Weinstein, 1999), and more recently, in the application of optimal control theory to time-dependent recovery from a perturbation (Weinstein, 2004). The delay in advancing from steady-state to time-dependent problems was due to the work needed to transform the linearized problem (a mix of differential and linear equations) into a dynamical system (Weinstein, 2004). The present work confirms the observation that the
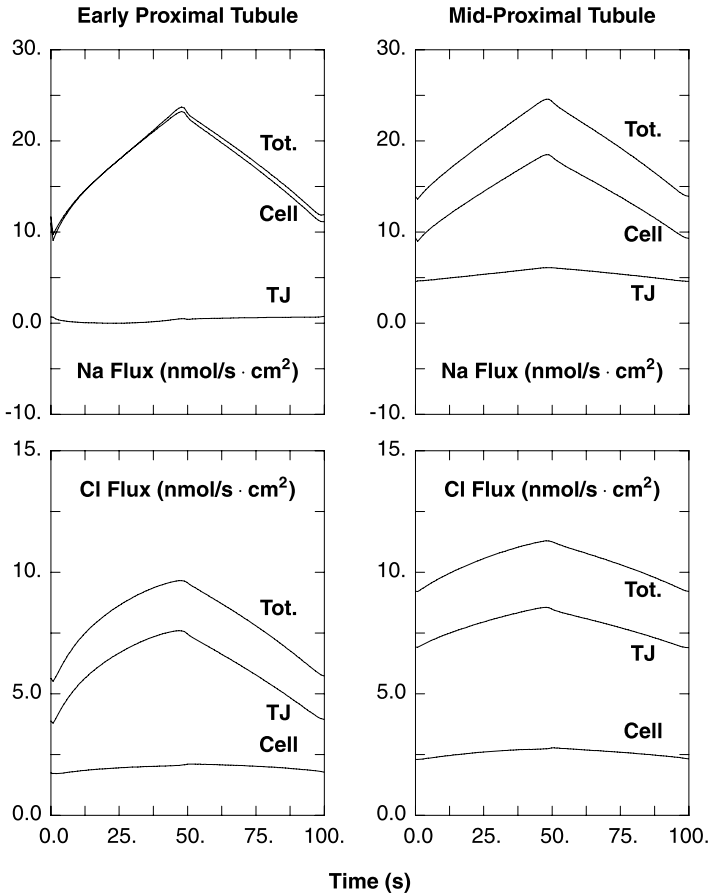
Fig. 10 Overall epithelial Na^+ and Cl^- fluxes during the tracking of luminal cell membrane Na^+ flux. For the tracking problem of Fig. 8, upper panels show whole epithelial Na^+ fluxes and lower panels Cl^- fluxes (Tot), as a sum of transcellular (Cell) and tight junctional (TJ) components. Panels on the left correspond to early luminal conditions; on the right to mid-proximal composition. The change is transcellular Na^+ flux was the tracking signal. This occurs with virtually no change in the transcellular component of Cl^- flux.

dynamical system appears to be sufficiently accurate to represent physiologically meaningful disturbances from the reference condition. Transitioning between the dynamical system and the physiological system introduces a significant level of complexity to the approach of this work. Nevertheless, the ability to generate coordinated control of multiple transporters is a substantial payoff, and while certainly not proof of physiological control, yields plausible, testable hypotheses regarding the early activation of both luminal and peritubular membrane transporters (vide infra).

In the present work, more attention has been given to formulating cost functions for the dynamical system. Beyond controlling a state variable, or the norm of the state variable vector, the present work has taken advantage of the model linearization to esti-

mate luminal membrane Na^+ flux as a linear function of the state variables. With this estimate, one gains the ability to formulate problems in which flux is stabilized or, more importantly, flux can be modulated to track changes in luminal fluid flow. During normal kidney function, there are routinely wide swings in proximal tubule fluid flow and proportional changes in Na^+ reabsorption. This is "glomerulotubular balance", and has been documented since the inception of micropuncture (Walker et al., 1941; Schnermann et al., 1968). These flow-dependent changes in transport appear to occur in the absence of any substantial change in the volume of the proximal tubule cell (Tong Wang, personal communication), and this observation provides a major challenge for any epithelial model. Of note, proximal tubule fluid composition changes along the tubule: within the first quarter of the tubule length, almost all of the glucose has been reabsorbed, as has the majority of the HCO_3^-, leaving behind a more acidic, Cl^--rich solution. This axial alteration in luminal composition changes fluxes through all of the transporters (diminished glucose flux, enhanced Cl^- flux), and changes the estimate of Na^+ flux as a function of the state variables. In this work, the axial change has been addressed, in calculations utilizing a second set of model conditions, with a lumen composition suggestive of mid-proximal fluid. The second component to the trajectory cost is that assigned to parameter modulation. In the prior work, all parameter changes were weighted equally; here, fractional parameter changes get equal weight. The impact of this change has been to de-emphasize the potential role of phosphate transport in cell homeostasis. Since the force for cellular phosphate uptake is substantial, but the flux is small, its transport permeability is also small. A cost function that had counted absolute parameter changes yielded a controller that had taken advantage of the large phosphate driving force to modulate cell volume.

The optimal control problem considered here has utilized state control. This provides a 24×9 feedback matrix for the dynamical system, or a 24×31 feedback matrix for the physiological system. With respect to the physiology of the proximal tubule cell, it is unlikely that such an abundance of potential controllers are available. Here and in the prior work, to export feedback to the physiological system, only controllers utilizing cell volume, peritubular membrane electrical potential, or the cellular concentrations of Na^+ (a surrogate for cell Ca^{++}) or HCO_3^- were considered admissible. The present work examined this practice with a calculation in the dynamical system: optimal state control was exported to the physiological system, restricted to the admissible subspace, and then translated back to the dynamical system (Figs. 6a and 6b). Back in the dynamical system, this subspace-restricted controller was compared with full state control, and at least in some problems, not a lot was lost. Indeed, direct examination of the full 24×31 feedback matrix showed that all but three of the columns had uniformly small entries, and these columns corresponded to cell volume, peritubular membrane electrical potential, and lateral interspace hydrostatic pressure. Furthermore, not all controllers were important for all problems: defense of cell volume utilized volume-dependent transporters, but little else; and defense of cell pH or Na^+ flux utilized peritubular membrane electrical potential and lateral interspace pressure, but not cell volume. It is curious that pH-dependent (equivalently HCO_3^--dependent) mechanisms were not selected for defense of cytosolic HCO_3^- concentration.

The basic issue raised by model identification of "optimal" (or less stringently, "useful") feedback controllers, is whether they actually exist. With respect to studies in proximal tubule, only two maneuvers have been used to increase cell volume: osmotic shock

(placing an isolated perfused tubule into a hypo-osmolar bathing solution), and tubule perfusion with organic solutes (glucose and amino acids), whose cellular uptake is Na^+-dependent. Only the latter maneuver produces an increase in reabsorptive Na^+ flux, and an early observation in rabbit proximal tubule was that luminal organics increased both overall Na^+ reabsorption and cell volume (Burg et al., 1976). Depending upon composition and concentration of the organics, the increase in Na^+ flux was in the range of 10%–50%. Subsequently, it was documented that this perfusion also depolarized the peritubular cell membrane (Beck and Potts, 1990) and alkalinized the tubule cell (Beck et al., 1993). Changes in peritubular transporters were studied electrophysiologically when luminal perfusion with organics increased cell volume by 23% (Breton et al., 1996). In these experiments, the peritubular K^+ conductance increased by 43%, the Cl^- conductance increased by a factor of 3.7, and there was little effect on Na^+–$3HCO_3$ permeability. The change in peritubular K^+ conductance followed the cell volume change with a delay, suggesting an indirect activation, rather than stretch per se. The first patch clamp study of the perfused proximal tubule, had revealed that this increase in K^+ conductance was due to an increase in open probability of peritubular K^+ channels (Beck et al., 1993). Of note, the 2-fold fractional change in K^+ conductance, relative to the fractional change in cell volume, observed by Breton et al. (1996), is comparable to the sensitivity of peritubular K^+ permeability ($HIS(K^+)$) to changes in the cytosolic impermeant ($C_1(Imp)$) predicted by the optimization calculations of the present model (Tables 3a and 3b, columns 3).

More generally, with respect to volume-dependent transporters, model identification of swelling-activated K^+-channels and K^+–Cl^- cotransporters, and shrink-activated Na^+/H^+ exchange reiterates known physiology (Lang et al., 1998a, 1998b). Shrink-activated Na^+–glucose transport, identified by the model, has not been documented experimentally, but does parallel known activation of coupled Na^+–amino acid transporters. There is considerably more uncertainty regarding the voltage-dependent transporters identified by the model: depolarization activation of the peritubular K^+ channel, and depolarization inactivation of Na^+–glucose, Na^+/H^+, and Na^+–$3HCO_3^-$ are all predicted to be useful to stabilization of cell HCO_3^- and luminal Na^+ flux. For the electrogenic cotransporters without any regulation, Na^+–glucose and Na^+–$3HCO_3^-$, depolarization would normally decrease throughput, and the optimal controller asks that this effect be amplified. For the peritubular K^+ channel of proximal tubule, there is little information on its regulation, but in general, voltage-dependent K^+ channels are not well represented within the kidney. With respect to the Na^+/H^+ exchanger, there is good evidence from vesicle transport studies that its flux rate is not voltage sensitive (Kinsella and Aronson, 1980). It is certainly possible that not all useful regulators are present in proximal tubule, but what should also be acknowledged is the possibility of depolarization–activation of a secondary signal (e.g. depolarization-induced Ca^{++} entry) that can act rapidly to activate a K^+ channel or inactivate a cotransporter. Such a short cascade would certainly be consistent with model prediction.

What was surprising to note in the feedback control matrix was the suggestion that increases in lateral intercellular space hydrostatic pressure should have the same regulatory effect as peritubular membrane depolarization. Conversely, decreases in interspace pressure should increase exit via the peritubular Na^+–$3HCO_3^-$ cotransporter and increase entry via luminal Na^+/H^+ and Na^+–glucose pathways; it should also diminish peritubular K^+ permeability. This is an intriguing observation because it was an unanticipated product of the model, and because its prediction parallels an extensive exper-

imental literature documenting the effect of peritubular protein concentration to regulate proximal tubule Na^+ flux (reviewed by Earley and Schrier, 1973; Weinstein, 2007). The ability to reverse the natriuresis of volume expansion with albumin infusion suggested that peritubular oncotic pressure could influence sodium reabsorption, and Earley and his associates (Earley et al., 1966; Martino and Earley, 1967) had proposed that renal interstitial pressure might be an intermediate variable. Subsequent micropuncture experiments in the rat documented peritubular protein enhancement of proximal sodium reabsorption (Brenner et al., 1969; Brenner and Troy, 1971; Knox et al., 1973; Green et al., 1974). A comparable effect was also observed in rabbit proximal convoluted tubule perfused in vitro (Imai and Kokko, 1974), and more recently in mouse tubules (Du et al., 2006). The critical feature of this scheme is that the action of peritubular protein is mediated through renal interstitial pressure and hence, pressures within the lateral intercellular spaces. The downstream effect of perturbing lateral interspace hydrostatic pressure has been a point of intense experimental interest. Based on micropuncture studies in the rat, Lewy and Windhager (1968) advanced the hypothesis that elevated interspace pressure would produce backflux of the sodium already transported into the interspace, across the tight junction and back into the lumen. This scheme was represented in a proximal tubule model by including a compliant tight junction (that would open in response to increases in interspace hydrostatic pressure), and the effect of peritubular Starling forces (data of Green et al., 1974) could be simulated, albeit at the cost of an extremely permeable tight junction (Weinstein, 1990). Notwithstanding the impact of physical factors on the paracellular pathway, there is evidence for an effect of volume expansion on the cell itself. Proximal tubule micropuncture documented decreased capacity for glucose reabsorption during volume expansion (Baines, 1971) and the correlation of proximal sodium and glucose reabsorption under the influence of albumin infusion (Kawamura et al., 1977). The case for a cellular effect of peritubular protein has also been presented by Berry and associates, who found depression of chloride reabsorption by isolated perfused tubules with removal of bath protein (Berry and Cogan, 1981; Baum and Berry, 1985). Pitts et al. found that volume expansion of the rabbit depressed phosphate transport in proximal straight tubules, as well as in brush border membrane vesicles (Pitts et al., 1988). At this time, a specific mechanism by which lateral interspace pressures could modulate transporter density has not been put forward, and this aspect of transport regulation has received little recent attention.

The tracking problem provides an important extension to identification of optimal feedback for recovery. The problem considered here was to vary transcellular Na^+ flux over a factor of two, with only trivial perturbation of cell volume and HCO_3^- concentration. With the tracking problem, there is provision for autonomous parameter modulation that is not contingent upon a state variable, and in the solution of the problem under consideration, both this autonomous term and the feedback terms were substantial. Furthermore, the model predicted that for each term, there would be modulation of both luminal and peritubular transport activity. At the peritubular membrane, increases in Na^+ transport engendered increases in the density of Na^+–$3HCO_3^-$ and K^+–Cl^- cotransporters, as well as in the Na^+, K^+–ATPase ion pump. This change in pump density would not have been suspected from feedback considerations alone. Conversely, with respect to the peritubular K^+ channel, the model predicted cancellation of both autonomous and feedback terms, so that there was virtually no change in this pathway through the variation in Na^+ flux (especially for mid-proximal conditions, Fig. 9b). At the luminal membrane, the

augmented Na$^+$ throughput was facilitated by increases in both the Na$^+$/H$^+$ exchanger and the Na$^+$–glucose cotransporter. Of note, model predictions included no significant change in the luminal membrane pathways for Cl$^-$ uptake, although at the whole epithelial level, changes in transepithelial electrical potential and in tight junction convection did vary Cl$^-$ reabsorption in parallel to that of Na$^+$. Ultimately, the relative contribution of Na$^+$–HCO$_3^-$ and Na$^+$–Cl$^-$reabsorption that would be produced by the controller of this tracking problem would need to be examined in a full tubule model.

The prediction of this model, of autonomous changes in luminal and peritubular transporter density, echoes the conclusion drawn in a recent attempt to directly model flow-dependent transport by rat proximal tubule (Weinstein et al., 2007). Beginning with the work of Guo et al. (2000), the hypothesis has been advanced that changes in luminal flow velocity vary the drag on luminal membrane microvilli, and that the internal actin filaments of the microvilli transmit this signal to the underlying actin cytoskeleton. In this scheme, an increase in microvillous torque will produce insertion of new transporters. This hypothesis has had experimental confirmation (Du et al., 2004, 2006), but thus far, direct evidence exists only for increases in luminal membrane Na$^+$/H$^+$ exchanger and in luminal membrane H$^+$–ATPase activities. The model by Weinstein et al. (2007) was an effort to represent flow-dependent transport in proximal tubule, as an epithelial model and also when configured as a tubule. The most important conclusion of that work was the prediction that luminal flow must activate both luminal and peritubular transporters. Increases in luminal membrane Na$^+$/H$^+$ exchange, or even in all of the luminal membrane transporters, produced only trivial increases in overall Na$^+$ flux or else produced massive derangement of cell volume. In that model, it was elected to increase the density of all transporters indiscriminately, in response to increases in luminal flow. The underlying biophysical assumption was that forces on the luminal cytoskeleton were transmitted instantaneously to the peritubular cytoskeleton, and as at the luminal membrane, produced insertion of new transporters. With that assumption, flow-dependent transport was achieved with no change in cell volume or composition. The present work sharpens the model of Weinstein et al. (2007), by considering selective changes in transporter density, on both luminal and peritubular cell membranes, computed as the solution of an optimal control problem.

For over two decades, Schultz and coworkers have investigated coordinated transport, or membrane "cross-talk" in intestinal epithelia. In their system, the prototypical event was the sudden introduction of luminal glucose and amino acids, and they observed cell swelling, increased Na$^+$ flux, and then after some delay, increased peritubular K$^+$ conductance (Gunter-Smith et al., 1982; Grasset et al., 1983; Lau et al., 1984), and this work prefigured similar studies in proximal tubule. Subsequently, these workers obtained evidence that an intact cytoskeleton was required for the signal to increase K$^+$ conductance, and that it could be activated in basolateral membrane vesicles, i.e. in the absence of changes in cytosolic composition (Dubinsky et al., 1999). Ultimately, Schultz concluded that "… membrane-stretch, secondary to cell swelling, brings about a disorganization of the actin cytoskeleton … and results in activation of the K$^+$ channel …" (Schultz and Dubinsky, 2001). Although volume-dependent modulation of membrane transporters has been demonstrated in proximal tubule, what this work adds to the discussion is the suggestion that activation of the actin cytoskeleton by luminal flow, rather than as a feedback response to derangement of cell volume, could provide a mechanism for enhancing cellular homeostasis during variations in glomerular filtration.

Acknowledgement

References

Alpern, R.J., Cogan, M.G., Rector, F.C. Jr., 1983. Flow dependence of proximal tubular bicarbonate absorption. Am. J. Physiol. 245, F478–F484.

Baines, A.D., 1971. Effect of extracellular fluid volume expansion on maximum glucose reabsorption rate and glomerular tubular balance in single rat nephrons. J. Clin. Invest. 50, 2414–2425.

Baum, M., Berry, C.A., 1985. Peritubular protein modulates neutral active NaCl absorption in rabbit proximal convoluted tubule. Am. J. Physiol. 248, F790–F795.

Beck, J.S., Hurst, A.M., Lapointe, J.-Y., Laprade, R., 1993. Regulation of basolateral K channels in proximal tubule studied during continuous microperfusion. Am. J. Physiol. 264, F496–F501.

Beck, J.S., Potts, D.J., 1990. Cell swelling, co-transport activation and potassium conductance in isolated perfused rabbit kidney proximal tubules. J. Physiol. 425, 369–378.

Berry, C.A., Cogan, M.G., 1981. Influence of peritubular protein on solute absorption in the rabbit proximal tubule. A specific effect on NaCl transport. J. Clin. Invest. 68, 506–516.

Brenner, B.M., Falchuk, K.H., Keimowitz, R.I., Berliner, R.W., 1969. The relationship between peritubular capillary protein concentration and fluid reabsorption by the renal proximal tubule. J. Clin. Invest. 48, 1519–1531.

Brenner, B.M., Troy, J.L., 1971. Postglomerular vascular protein concentration: Evidence for a causal role in governing fluid reabsorption and glomerulotubular balance by the renal proximal tubule. J. Clin. Invest. 50, 336–349.

Breton, S., Marsolais, M., Lapointe, J.Y., Laprade, R., 1996. Cell volume increases of physiologic amplitude activate basolateral K and Cl conductances in the rabbit proximal convoluted tubule. J. Am. Soc. Nephrol. 7, 2072–2087.

Burg, M.B., Patlak, C., Green, N., Villey, D., 1976. Organic solutes in fluid absorption by renal proximal convoluted tubules. Am. J. Physiol. 231, 627–637.

Chan, Y.L., Biagi, B., Giebisch, G., 1982. Control mechanisms of bicarbonate transport across the rat proximal convoluted tubule. Am. J. Physiol. 242, F532–F543.

Du, Z., Duan, Y., Yan, Q., Weinstein, A.M., Weinbaum, S., Wang, T., 2004. Mechanosensory function of microvilli of the kidney proximal tubule. Proc. Natl. Acad. Sci. 101, 13068–13073.

Du, Z., Yan, Q., Duan, Y., Weinbaum, S., Weinstein, A.M., Wang, T., 2006. Axial flow modulates proximal tubule NHE3 and H–ATPase activities by changing microvillous bending moments. Am. J. Physiol. 290, F289–F296.

Dubinsky, W.P., Mayorga-Wark, O., Schultz, S.G., 1999. Volume regulatory responses of basolateral membrane vesicles from Necturus enterocytes: Role of the cytoskeleton. Proc. Natl. Acad. Sci. 96, 9421–9426.

Earley, L.E., Martino, J.A., Friedler, R.M., 1966. Factors affecting sodium reabsorption by the proximal tubule as determined during blockade of distal sodium reabsorption. J. Clin. Invest. 45, 1668–1684.

Earley, L.E., Schrier, R.W., 1973. Intrarenal control of sodium excretion by hemodynamic and physical factors. In: Orloff, J., Berliner, R.W. (Eds.), Handbook of Physiology. Sect. 8: Renal Physiology, pp. 721–762. American Physiological Society, Washington.

Gertz, K.H., Boylan, J.W., 1973. Glomerular-tubular balance. In: Orloff, J., Berliner, R.W. (Eds.), Handbook of Physiology. Section 8: Renal Physiology, pp. 763–790. American Physiological Society, Washington.

Grasset, E., Gunter-Smith, P., Schultz, S.G., 1983. Effects of Na-coupled alanine transport on intracellular K activities and the K conductance of the basolateral membranes of Necturus small intestine. J. Membr. Biol. 71, 89–94.

Green, R., Moriarty, R.J., Giebisch, G., 1981. Ionic requirements of proximal tubular fluid reabsorption: Flow dependence of fluid transport. Kidney Int. 20, 580–587.

Green, R., Windhager, E.E., Giebisch, G., 1974. Protein oncotic pressure effects on proximal tubular fluid movement in the rat. Am. J. Physiol. 226, 265–276.

Gunter-Smith, P.J., Grasset, E., Schultz, S.G., 1982. Sodium-coupled amino acid and sugar transport by *Necturus* small intestine. An equivalent electrical circuit analysis of a rheogenic co-transport system. J. Membr. Biol. 66, 25–39.

Guo, P., Weinstein, A.M., Weinbaum, S., 2000. A hydrodynamic mechanosensory hypothesis for brush border microvilli. Am. J. Physiol. 279, F698–F712.

Haberle, D.A., von Baeyer, H., 1983. Characteristics of glomerulotubular balance. Am. J. Physiol. 244, F355–F366.

Imai, M., Kokko, J.P., 1974. Transtubular oncotic pressure gradients and net fluid transport in isolated proximal tubules. Kidney Int. 6, 138–145.

Kawamura, J., Mazumdar, D.C., Lubowitz, H., 1977. Effect of albumin infusion on renal glucose reabsorption in the rat. Am. J. Physiol. 232, F286–F290.

Kinsella, J.L., Aronson, P.S., 1980. Properties of the Na^+–H^+ exchanger in renal microvillus membrane vesicles. Am. J. Physiol. 238, F461–F469.

Kleinman, D.L., 1968. On an iterative technique for Riccati equation computations. IEEE Trans. Autom. Control 13, 114–115.

Knight, T.F., Senekjian, H.O., Sansom, S.C., Weinman, E.J., 1980. Proximal tubule glucose efflux in the rat as a function of delivered load. Am. J. Physiol. 238, F499–F503.

Knox, F.G., Schneider, E.G., Willis, L.R., Strandhoy, J.W., Ott, C.E., 1973. Effect of volume expansion on sodium excretion in the presence and absence of increased delivery from superficial proximal tubules. J. Clin. Invest. 52, 1642–1646.

Lang, F., Busch, G.L., Ritter, M., Volkl, H., Waldegger, S., Gulbins, E., Haussinger, X., 1998a. Functional significance of cell volume regulatory mechanisms. Physiol. Rev. 78, 247–306.

Lang, F., Busch, G.L., Volkl, H., 1998b. The diversity of volume regulatory mechanisms. Cell. Physiol. Biochem. 8, 1–45.

Lau, K.R., Hudson, R.L., Schultz, S.G., 1984. Cell swelling increases a barium-inhibitable potassium conductance in the basolateral membrane of *Necturus* small intestine. Proc. Natl. Acad. Sci. 81, 3591–3594.

Lewy, J.E., Windhager, E.E., 1968. Peritubular control of proximal tubular fluid reabsorption in the rat kidney. Am. J. Physiol. 214, 943–954.

Liu, F.-Y., Cogan, M.G., 1988. Flow dependence of bicarbonate transport in the early (S_1) proximal convoluted tubule. Am. J. Physiol. 254, F851–F855.

Maddox, D.A., Fortin, S.M., Tartini, A., Barnes, W.D., Gennari, F.J., 1992. Effect of acute changes in glomerular filtration rate on Na^+/H^+ exchange in rat renal cortex. J. Clin. Invest. 89, 1296–1303.

Martino, J.A., Earley, L.E., 1967. Demonstration of a role of physical factors as determinants of the natriuretic response to volume expansion. J. Clin. Invest. 46, 1963–1978.

Pitts, T.O., McGowan, J.A., Chen, T.C., Silverman, M., Rose, M.E., Puschett, J.B., 1988. Inhibitory effects of volume expansion performed in vivo on transport in the isolated rabbit proximal tubule perfused in vitro. J. Clin. Invest. 81, 997–1003.

Preisig, P.A., 1992. Luminal fbw rate regulates proximal tubule H–HCO_3 transporters. Am. J. Physiol. 262, F47–F54.

Romano, G., Favret, G., Damato, R., Bartoli, E., 1998. Proximal reabsorption with changing tubular fluid inflow in rat nephrons. Exp. Physiol. 83, 35–48.

Schnermann, J., Wahl, M., Liebau, G., Fischbach, H., 1968. Balance between tubular fbw rate and net fluid reabsorption in the proximal convolution of the rat kidney. Pflugers Arch. 304, 90–103.

Schultz, S.G., 1981. Homocellular regulatory mechanisms in sodium-transporting epithelia: Avoidance of extinction by "flush-through". Am. J. Physiol. 241, F579–F590.

Schultz, S.G., 1992. Membrane cross-talk in sodium-absorbing epithelial cells. In: Seldin, D.W., Giebisch, G. (Eds.), The Kidney. Physiology and Pathophysiology, pp. 287–299. Raven, New York, Chap. 11.

Schultz, S.G., Dubinsky, W.P., 2001. Sodium absorption, volume control and potassium channels: in tribute to a great biologist. J. Membr. Biol. 184, 255–261.

Sontag, E., 1998. Mathematical Control Theory. Deterministic Finite Dimensional Systems, 2nd edn. Springer, New York, pp. 1–531.

Walker, A.M., Bott, P.A., Oliver, J., MacDowell, M.C., 1941. The collection and analysis of fluid from single nephrons of the mammalian kidney. Am. J. Physiol. 134, 580–595.

Weinstein, A.M., 1983. A non-equilibrium thermodynamic model of the rat proximal tubule epithelium. Biophys. J. 44, 153–170.

Weinstein, A.M., 1985. Glucose transport in a model of the rat proximal tubule epithelium. Math. Biosci. 76, 87–115.

Weinstein, A.M., 1990. Glomerulotubular balance in a mathematical model of the proximal nephron. Am. J. Physiol. 258, F612–F626.

Weinstein, A.M., 1992. Chloride transport in a mathematical model of the rat proximal tubule. Am. J. Physiol. 263, F784–F798.

Weinstein, A.M., 1994. Ammonia transport in a mathematical model of the rat proximal tubule. Am. J. Physiol. 267, F237–F248.

Weinstein, A.M., 1995. A kinetically defined Na^+/H^+ antiporter within a mathematical model of the rat proximal tubule. J. Gen. Physiol. 105, 617–641.

Weinstein, A.M., 1996. Coupling of entry to exit by peritubular K^+-permeability in a mathematical model of the rat proximal tubule. Am. J. Physiol. 271, F158–F168.

Weinstein, A.M., 1999. Modeling epithelial cell homeostasis: Steady-state analysis. Bull. Math. Biol. 61, 1065–1091.

Weinstein, A.M., 2004. Modeling epithelial cell homeostasis: Assessing recovery and control mechanisms. Bull. Math. Biol. 66, 1201–1240.

Weinstein, A.M., 2007. Sodium and chloride transport: Proximal nephron. In: Alpern, R.J., Hebert, S.C. (Eds.), Seldin and Giebisch's The Kidney: Physiology and Pathophysiology, 4th edn. pp. 793–848. Elsevier, Amsterdam, Chap. 30.

Weinstein, A.M., Weinbaum, S., Duan, Y., Du, Z., Yan, Q., Wong, T., 2007. Flow-dependent transport in a mathematical model of rat proximal tubule. Am. J. Physiol. 292, F1164–F1181.

Wilcox, C.S., Baylis, C., 1985. Glomerular-tubular balance and proximal regulation. In: Seldin, D.W., Giebisch, G. (Eds.), The Kidney. Physiology and Pathophysiology, pp. 985–1012. Raven, New York.

Wong, K.R., Berry, C.A., Cogan, M.G., 1995. Flow dependence of chloride transport in rat S1 proximal tubules. Am. J. Physiol. 269, F870–F875.

Wonham, W.M., 1985. Linear Multivariable Control: A Geometric Approach. Springer, New York, pp. 1–334.